PLATE AND COLUMN EFFICIENCIES FOR RECTIFYING COLUMN

BY

KAKUSABURO ONDA and KATSUROKU TAKAHASHI

Department of Chemical Engineering

CONTENTS

Page

Chapter 1. Introduction 141
Chapter 2. Definition of plate efficiency $(E_{MV})_{1/2}$ 142
2.1. For plug flow of liquid on a plate 142
2.2. Relation between plate and point efficiencies under consideration of liquid mixing on the plate. 144
Chapter 3. Empirical correlation of plate efficiencies $(E_{MV})'_{1/2}$ 146
Chapter 4. Calculation of theoretical number of plate in distillation column 148
4.1. Calculation for plug flow of liquid on plate 148
4.1.1. Graphical method 148
4.1.2. Minimum number of theoretical plates 149
4.1.3. Relation between column efficiency and plate efficiency 150
4.2. Consideration of liquid mixing on the plate 153
4.2.1. Graphical method 153
4.2.2. Relation between $(E_{MV})'_{1/2}$ and $(E_{MV})_{1/2}$ 156
4.2.3. Relation between column efficiency and plate efficiency 157
4.2.4. Relation between $(E_{ML})_{1/2}$ and $(E_{MV})_{1/2}$ 161
4.3. Calculation for multicomponent system 162
4.3.1. Graphical method for ternary system 162
4.3.2. Step-to-step calculation 163
4.3.3. Effect of liquid mixing on number of plates 164
Chapter 5. Eddy diffusivity in liquid on plate 165
5.1. Experiments 165
5.2. Effects of operating and design variables on eddy diffusivity 166
5.3. Effect of physical properties on eddy diffusivity 169
Chapter 6. Effect of phase change on plate efficiency 171
6.1. Heat transfer coefficient for condensation 171
6.2. Mass transfer coefficients for mixed vapor condensation 176
6.3. Effect of phase change on point efficiency 178

Chapter 1. Introduction

The distillation with the plate column is most commonly used as the seperation process in industry. In the design of the distillation column, the plate efficiency plays an important role. The plate efficiency has been defined as Murphree's plate efficiency with the vapor composition in equilibrium with the liquid leaving the plate. This efficiency is reasonable only when the liquid on the plate is well mixed and there is no composition gradient in liquid. In practice, however, the liquid

composition will vary as the liquid flows on the plate. In the case of larger columns and systems with high relative volatility, Murphree's plate efficiencies have been found to be more than 100%. Furthermore, as described in the later section, this plate efficiency decrease with the increase of reflux ratio for a constant point efficiency.

In this article, a modified plate efficiency is newly defined with a rational assumption that the vapor on the ideal plate is in equilibrium with the liquid at the center of the plate. The relations between the plate and point efficiencies are discussed and the plate efficiencies are correlated with the operating variables, the design variables and the physical properties.

Under the same assumption of ideal plate as used in the definition of the plate efficiency, the method to calculate the number of plates, the relation between the column and plate efficiencies and so on, are derived. With the usual condition of distillation the liquid mixing little influences on the plate efficiency newly defined, but it plays an important role in the calculation of the number of plates. Then, the eddy diffusivities in the liquid on the bubble-cap plates are measured with the tracer technique and they are correlated with the operating and design variables. In addition, the effects of physical properties on the eddy diffusivities are discussed.

The plate efficiency has been usually investigated only from the viewpoint of mass transfer as the distillation is an adiabatic process. In practice, however, the temperature of liquid differs from plate to plate, and the condensation and vaporization are repeated at a local point in vapor-liquid contacting layer. In other wards, the mass transfer process on the plate is accompanied with the phase change caused by the heat transfer. The effects of phase change on the plate efficiency are considered from the results of the mixed vapor condensation in a wetted wall column.

Chapter 2. Definition of plate efficiency $(E_{MV})_{1/2}$

2. 1. For plug flow of liquid on a plate

The conception of efficiency in the distillation column had been first clarified in the 1920's, and Lewis, Jr.[1] gave the fundamentals of the point, plate and column efficiencies which are used now in general. Many investigations on these efficiencies have been carried out after that time. Author *et al.*[2~5] explained the history of plate efficiency in detail. On the problem of plate efficiency we started from the correction of irrationality in the material balance for the derivation of relation between the plate and point efficiencies, which appeared in "Application of Differencial Equations" by Marshall-Pigford.[6] When liquid flows on the plate as a plug flow, Murphree's plate efficiency $(E_{MV})_1$ based on the vapor composition in equilibrium with liquid leaving the plate decreases considerably with the decrease of λ, that is, the increase of reflux ratio for a constant point efficiency as shown in Fig. 1. These results are in contradiction to the common sense. On the other hand, the plate efficiency $(E_{MV})_0$ based on the vapor composition in equilibrium with liquid entering the plate increases with the increase of reflux ratio as shown in Fig. 2. Thus, the plate efficiencies vary largely with liquid composition chosen at any point on a plate.

Therefore, author[7] proposed the modified plate efficiency based on the vapor composition in equilibrium with liquid at the center of plate as given by:

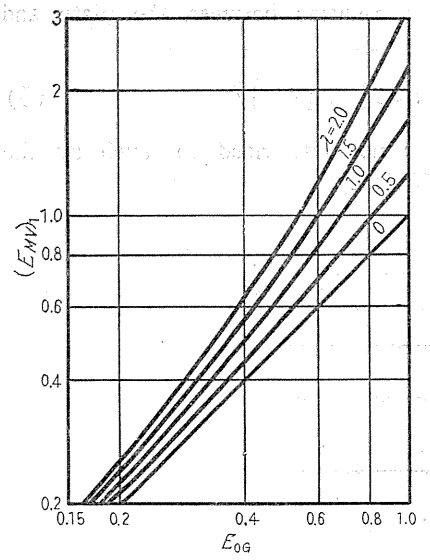

Fig. 1. Correlation of $(E_{MV})_1$ and E_{OG} with λ as a parameter.

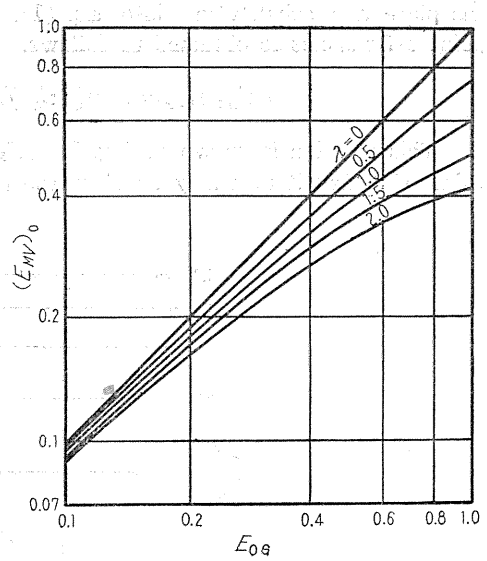

Fig. 2. Correlation of $(E_{MV})_0$ and E_{OG} with λ as a parameter.

$$(E_{MV})_{1/2}=\frac{(y_n)_{av}-y_{n-1}}{(y_n^*)_{1/2}-y_{n-1}} \tag{1}$$

where $(y_n)_{av}$ is mean vapor composition on n-th plate, y_{n-1} the vapor composition on (n-1)th plate assuming the vapor from the under plate is completely mixed, and $(y_n^*)_{1/2}$ the vapor composition in equilibrium with liquid at the center of plate.

Material balance for the differential section dw $(=dz/dZ)$ in the direction of liquid flow on a plate is written as:

$$Lx_n+(Vdw)y_{n-1}=L(x_n+dx_n)+(Vdw)y_n \tag{2}$$

where z and Z are the distances from inlet weir to arbitrary point on the plate and from inlet to outlet weir respectively, L and V are the flow rates [kg-mole/hr] of liquid and vapor, and x_n is the liquid composition on n-th plate. Under an assumption of a linear equilibrium line $y^*=mx+b$, Eq. (2) is arranged as:

$$(y_n-y_{n-1})\lambda=dy^*/dw \tag{3}$$

where $\lambda=mV/L$. By using the definition of the point efficiency E_{OG}, y_n^* is eliminated from Eq. (3) as follows.

$$(y_n/dw)+\lambda E_{OG}y_n=\lambda E_{OG}y_{n-1} \tag{4}$$

With the boundary condition, $y_n=(y_n)_{1/2}$ at $w=1/2$, Eq. (4) is solved, and then the solution is given by:

$$y_n=y_{n-1}+\{(y_n)_{1/2}-y_{n-1}\}exp\{\lambda E_{OG}(0.5-w)\} \tag{5}$$

The average vapor composition on the plate is obtained by integrating Eq. (5) over

the plate and substituting into Eq. (1). Then, a relation between the plate and point efficiencies is obtained as follows.

$$(E_{MV})_{1/2}=exp(\lambda E_{OG}/2)\{1-exp(\lambda E_{OG}/2)\}/\lambda \quad (6)$$

This relation is shown in Fig. 3. $(E_{MV})_{1/2}$ is not influenced so much by the value of λ, and it is nearly equal to the point efficiency.

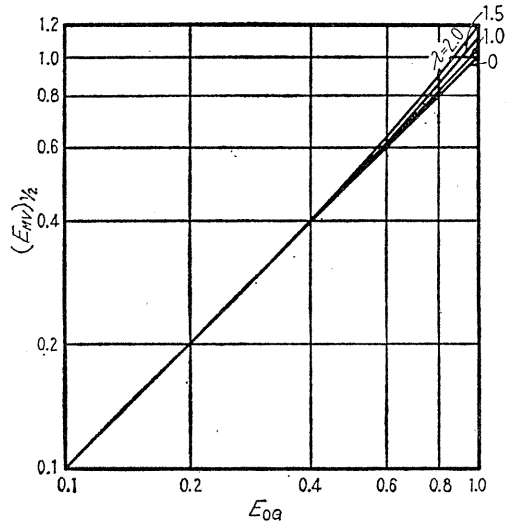

Fig. 3 Correlation of $(E_{MV})_{1/2}$ and E_{OG} with λ as a parameter.

2. 2. *Relation between plate and point efficiencies under consideration of liquid mixing on the plate*[8]

To express the liquid mixing on a plate, various models have been proposed[9~11]. Using the eddy diffusion model, the material barance for the differential section on a plate as shown in Fig. 4, is given as follows.

$$D_E A\rho_L(d^2x/dz^2)-L(y_{n-1}-y_n)(V/z)(dx/dz)=0 \quad (7)$$

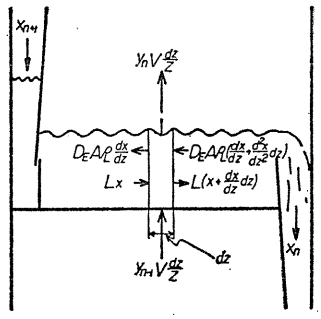

Fig. 4. Schematic diagram of a plate for material balance.

Where D_E is the eddy diffusivity [m²/hr], A the cross-sectional flow area of the liquid segment on the plate [m²], and ρ_L the liquid density [kg/m³]. Eq. (7) is rewritten in the dimensionless form as follows.

$$\{(d^2x/dw^2)/N_{Pe}\}-(dx/dw)-\lambda E_{OG}(x-x^*_{n-1})=0 \quad (8)$$

where N_{Pe} is Peclet's number $(=Z^2/D_E t_L)$, x^*_{n-1} the liquid composition in equilibrium with y_{n-1}, and t_L the contacting time of liquid with vapor [hr]. Boundary

conditions are given by:

$$x=x_n \text{ at } w=1/2 \text{ and } (dx/dw)=0 \text{ at } w=1 \tag{9}$$

Then, a solution of Eq. (8) is given as follows.

$$\frac{x-x^*_{n-1}}{x_n-x^*_{n-1}}=\frac{exp[(\eta+N_{Pe})\{w-(1/2)\}]}{1+\{(\eta+N_{Pe})/\eta\}exp\{\eta+(N_{Pe}/2)\}}$$

$$+\frac{exp[\{(\eta+N_{Pe})/2\}-\eta(w-1)]}{exp\{\eta+(N_{Pe}/2)\}+\{\eta/(\eta+N_{Pe})\}} \tag{10}$$

where

$$\eta=(N_{Pe}/2)\{\sqrt{1+(4\lambda E_{OG}/N_{Pe})}-1\} \tag{11}$$

The relation between the plate and point efficiencies is obtained by integrating Eq. (10) as follows.

$$\frac{(E_{MV})_{1/2}}{E_{OG}}=\int_0^1 \frac{x-x^*_{n-1}}{x_n-x^*_{n-1}}dw$$

$$=\frac{\{1-exp(-\eta-N_{Pe})\}exp\{(\eta+N_{Pe})/2\}}{(\eta+N_{Pe})[1+\{(\eta+N_{Pe})/2\}exp\{\eta+(N_{Pe}/2)\}]}$$

$$+\frac{\{exp(\eta)-1\}exp\{(\eta+N_{Pe})/2\}}{\eta[exp\{\eta+(N_{Pe}/2)\}+\{\eta/(\eta+N_{Pe})\}]} \tag{12}$$

For various values of N_{Pe}, $(E_{MV})_{1/2}/E_{OG}$ are drawn against λE_{OG} in Fig. 5. In this figure, $(E_{MV})_1/E_{OG}$ are also shown with broken lines. For a fixed value of

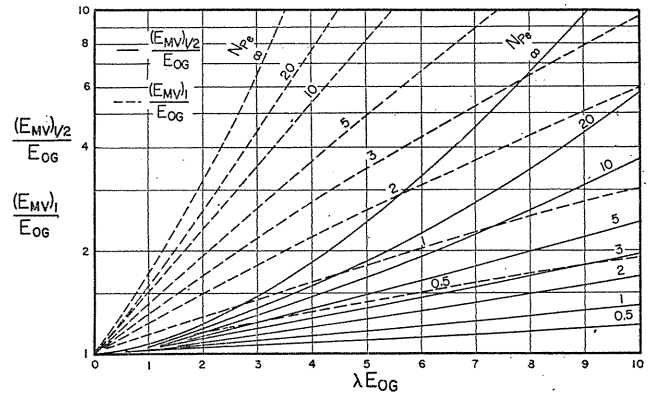

Fig. 5. Variation of $(E_{MV})_{1/2}/E_{OG}$ and $(E_{MV})_1/E_{OG}$ with λE_{OG} for various values of peclet's number N_{Pe}.

N_{Pe}, the variation of $(E_{MV})_{1/2}/E_{OG}$ with λ is much smaller than that of $(E_{MV})_1/E_{OG}$. In the case of $\lambda E_{OG}<1$ (this condition holds for almost all the practical columns), the value of $(E_{MV})_{1/2}/E_{OG}$ is less than 1.04 for any value of N_{Pe}, and

the following relation holds within 4% error.

$$(E_{MV})_{1/2}=E_{OG} \tag{13}$$

Therefore, the effect of liquid mixing on the plate efficiency need not be taken into account.

Chapter 3. Empirical correlation of plate efficiencies $(E_{MV})'_{1/2}$[12]

The modified plate efficiency has been defined by Eq. (1) with the vapor composition in equilibrium with liquid at the center of plate. However, it is practical to measure the composition of liquid at the outlet of plate. Thus, the mean of liquid compositions at the inlet and outlet of plate is used instead of the liquid composition at the center of plate. Then the plate efficiency is written as:

$$(E_{MV})'_{1/2}=\{(y_n)_{av}-y_{n-1}\}/\{(y^*_n)'_{1/2}-y_{n-1}\} \tag{14}$$

where $(y^*_n)'_{1/2}$ is the vapor composition in equilibrium with the liquid composition which is the mean value at the inlet and outlet of plate.

$(E_{MV})'_{1/2}$ calculated from data reported by Delaware Univ.[13] are plotted against L/V in Fig. 6. The value of $(E_{MV})'_{1/2}$ varies little with L/V, that is, the dependence of the plate efficiency $(E_{MV})'_{1/2}$ on the reflux ratio is very small. This is expected from the result shown in Fig. 5.

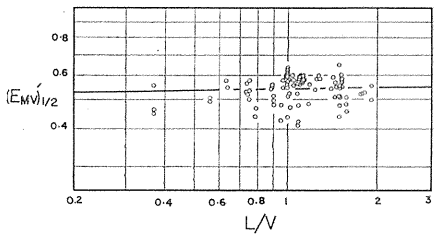

Fig. 6. Relation between modified plate efficiency $(E_{MV})'_{1/2}$ and L/V.

The variable affecting the plate efficiency of bubble-cap column can be divided into three main groups: system-property variables, operating variables, and plate-design variables. System-property variables depend upon the type and the composition of components. These are the relative volatility, the gas and liquid density, the viscosity and diffusivity, and the surface tention. Operating variables include the gas and liquid flow rates, the temperature, and the pressure. Plate-designs are the plate dimensions: the plate spacing, the weir height, and the design and arrangement of bubble caps.

The effects of these variables on the plate efficiency have already been studied [13~19]. Keeping these in mind, the dimensionless groups involving the important physical-property, design, and operating variables have been selected. They are, namely, Schmidt's number N_{ScL} $(=\mu_L/\rho_L D_L)$, capillary number N_{Ca} $(=\mu_V u_V/\sigma)$, Reynold's number of liquid N_{ReL} $(=4\Gamma/\mu_L)$, Reynold's number of vapor N_{ReV} $(=d_{sl}u_V\rho_V/\mu_V)$, relative volatility α, and design group $(Z\cdot h_w/Sa)$. Where μ is the viscosity [kg/m·sec], D_L the diffusivity of liquid [m²/hr], u_V the vapor velocity at the slot [m/hr], σ the surface tention [kg/m²], Γ the liquid flow rate [kg/m·hr], d_{sl} the equivalent diameter of slot [m], h_w the weir height [m], and Sa the sum of the area of all slots on a plate [m²].

Particular care has been taken in the selection of date. Accurately measured date are essential for the correlation study. Also, the effect of plate-design varia-

bles can be experienced only by a large-scale unit. The date of binary system with the composition of the consecutive plates have been reported for various systems, *i. e.*, acetone-benzene[13], *n*-pentane-*p*-xylene[13], methanol-toluene[14], and *i*-octane-toluene[20]. These efficiencies for the systems have been correlated with the dimensionless groups mentioned above by the least square method, and the following correlation is obtained.

$$((E_{MV})'_{1/2}=0.1359(N_{ReV})^{-0.192}(N_{ReL})^{0.242}(N_{ScL})^{0.095}$$
$$\times(N_{Ca})^{-0.085}(\alpha)^{-0.267}\left(\frac{Z\cdot h_w}{S_a}\right)^{0.076} \qquad (15)$$

This correlation is strictly applicable to a single plate of the column using binary systems. Eq. (15) expresses the experimental data of industrial scale columns quite satisfactorily with the standard deviation 0.0498 as shown in Fig. 7. By changing

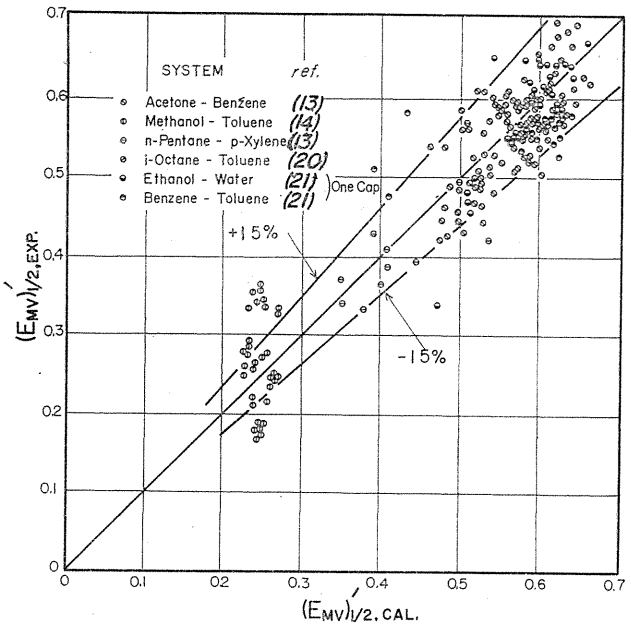

Fig. 7. Comparison of experimental values of plate efficiencies $(E_{mu})'_{1/2}$ and those calculated with Eq. (15).

the constant 0.1359 to 0.2699, $(E_{MV})'_{1/2}$ calculated by Eq. (15) agree with the experimental values[21] for the laboratory scale column with the standard deviation 0.054 as shown in Fig. 7.

In the same way as described above, Murphree's plate efficiencies $(E_{MV})_1$ have been correlated as Eq. (15)' in Fig. 8, with the coefficient and exponents different from those in Eq. (15). However, the standard deviation in this case is found to be 0.238. It is larger 4 times than that from the correlation of $(E_{MV})'_{1/2}$. The fact suggests that to correlate $(E_{MV})_1$ accurately is more difficult than to do $(E_{MV})'_{1/2}$.

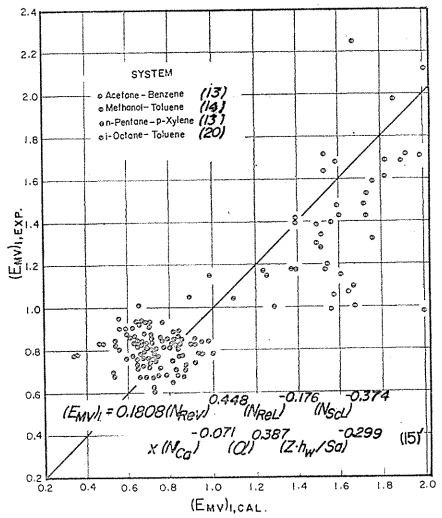

Fig. 8. Comparison of experimental values of Murphree's plate efficiencies $(E_{MV})_1$ and those calculated with Eq. (15)'.

Chapter 4. Calculation of theoretical number of plate in distillation column

4. 1. Calculation for plug flow of liquid on plate

4. 1. 1. Graphical method[12]

To determine the number of theoretical plates for the distillation column, McCabe-Thiele's method[22] is most commonly used. This method involves the stepwise construction between the operating lines and the equilibrium curve, assuming no composition gradient in liquid on the plate, and taking into account the vapor composition in equilibrium with liquid leaving the plate. In practice, however, the liquid composition varies from the inlet to outlet of plate. It is clear that the column diameter becomes larger, the composition difference in liquid becomes greater on the plate.

Taking into account the liquid composition gradient under the same assumption as used in the definition of the plate efficiency $(E_{MV})_{1/2}$ (*i. e.*, vapor on the ideal plate is in equilibrium with liquid at the center of plate), the method of stepwise construction for the plug flow of liquid is given as follows. With the assumption that the liquid and vapor flow rates are constant over the section of the column between feeds and top products, the material balance of a specified component for the system enclosed by the broken line in Fig. 9 is written as:

$$(y_{n-1}+y_n)/2=(L/V)x_n+(D/V)x_D \tag{16}$$

where x_n is the liquid composition at the center of n-th plate, and D and x_D the flow rate and composition of top products respectively. The plate numers are counted upward from the bottom to the top of the column. Eq. (16) represents the operating line for the enriching section. The operating line for the stripping section can be obtained similarly.

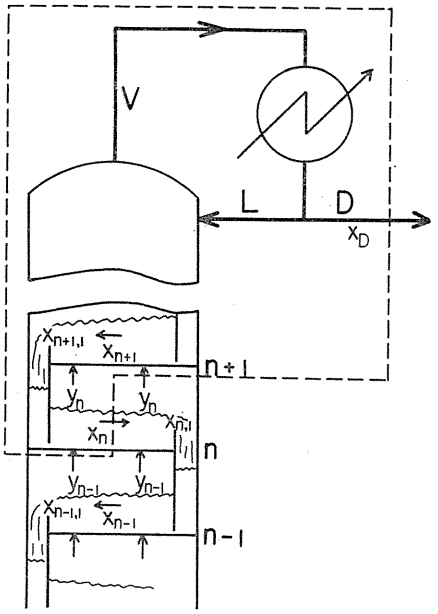

Fig. 9. Schematic diagram of rectifying section of continuous distillation column. The region bounded by broken line shows the system for material balance.

$$(y_{(n-1)^\circ}+y_{n^\circ})/2=(L'/V')x_{n^\circ}-(W/V')x_W \qquad (17)$$

where W and x_W are the flow rate and composition of bottom products, respectively. Also, for an ideal plate, vapor is assumed to be in equilibrium with liquid at the center of plate.

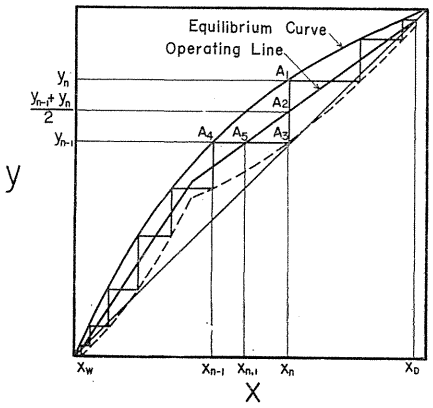

Fig. 10. Stepwise construction for plug flow of liquid on the plate.

$$y_n=f(x_n) \qquad (18)$$

For binary system, Eqs. (16) and (18) are expressed on x-y diagram as shown in Fig. 10. Then, the graphical procedure for n-th theoretical plate is expressed as follows. A vertical line from x_n is drawn to intersect the operating line at A_2 and the equilibrium curve at A_1. From Eq. (16), A_2 is expressed by $\{(y_{n-1}+y_n)/2, x_n\}$ and from Eq. (18) A_1 by (x_n, y_n). Then the point A_3, which gives the vapor composition y_{n-1} of (n-1)th plate, is determined by $\overline{A_1A_2}=\overline{A_2A_3}$. A horizontal line is drawn through A_3 so as to cut the operating line at A_5 $(y_{n-1}, x_{n,1})$ and the equilibrium curve at A_4 (y_{n-1}, x_{n-1}), where $x_{n,1}$ is the liquid composition at the outlet of plate. Drawing the locus of point A_3 which is given by $\overline{A_1A_2}=\overline{A_2A_3}$ as shown in Fig. 10 with the broken line, the theoretical number of plates is determined by the stepwise construction between the locus and equilibrium curve.

4. 1. 2. Minimnm nuber of theoretical plates[12]

With the assumption that the liquid on a plate is well mixed and hence its composition is uniform, the minimum number of theoretical plate has been given by Fenske.[23].

On the contrary, as it has been assumed here that liquid flows as an unidirectional plug flow on the plate, the following relation between the compositions of top and bottom products can be derived for the total reflux operation.

$$(x_{i,D}/x_{j,D})=\alpha_{ij}^{2(N+1)}(x_{i,W}/x_{j,W}) \qquad (19)$$

where

$$\alpha_{ij}^{2(N+1)}=\left\{\left(\frac{K_{i,(D,N)}}{K_{j,(D,N)}}\right)\left(\frac{K_{i,N}}{K_{j,N}}\right)\right\}\times\cdots\times\left\{\left(\frac{K_{i,(n,n-1)}}{K_{j,(n,n-1)}}\right)\left(\frac{K_{i,n-1}}{K_{j,n-1}}\right)\right\}$$
$$\times\cdots\times\left(\left\{\frac{K_{i,(1,w)}}{K_{j,(1,w)}}\right)\left(\frac{K_{i,w}}{K_{j,w}}\right)\right\} \tag{20}$$

In Eq. (20), $K_{i,(n,n-1)}$ is a mean value between $K_{i,n}$ and $K_{i,n-1}$, and $K_{i,n}$ the vapor-liquid equilibrium constant of i-component on n-th plate. By rearranging Eq. (19), the minimum number of theoretical plates is given approximately by:

$$S_m=N_m+1=[\log\{(x_{i,D}/x_{j,D})(x_{j,w}/x_{i,w})\}]/\{2(\log\alpha_{ij})\} \tag{21}$$

Thus, the minimum number of theoretical plates is nearly one half of that given by Fensk's equation under the assumptions just described.

4. 1. 3. Relation between column efficiency and plate efficiency[24]

The column efficiency, which is the ratio of the number of theoretical plates to that of practical plates, is important for the design of distillation column. However, there is no method to calculate the column efficiency exactly. For the case where the equilibrium curve can be represented by a straight line, the relation between the column efficiency and Murphree's plate efficiency $(E_{MV})_1$ has been given by Lewis, Jr.[1]

With the same assumption as Lewis (i. e., the equilibrium curve is a straight line and the plate efficiency is constant over the column), a relation between the column efficiency E_T and the plate efficiency $(E_{MV})_{1/2}$ defined by Eq. (1) is derived.

The equilibrium curve being a straight line is given by,

$$y_n=mx_n+b_1=(L/V)\lambda x_n+b_1 \tag{22}$$

and the operating line is expressed by

$$y=(L/V)x_n+(D/V)x_D \tag{23}$$

From Eqs. (16) and (23), $y=(y_{n-1}+y_n)/2$. Therefore, a line drawn symmetrically in y-direction for the equilibrium curve from the operating line is given by:

$$y_{n-1}=(L/V)(2-\lambda)x_n+\{2(D/V)x_D-b_1\} \tag{24}$$

Thus, the number of theoretical plates is determined by the stepwise construction between the lines expressed by Eqs. (22) and (24) as shown in Fig. 11.

Under the assumption that the plate efficiency is constant over the column, the number of practical plates is determined by the stepwise construction between lines (25) and (26) as shown in Fig. 11. If these two lines are expressed by:

$$y_{n'}=a_2x_{n'}+b_2 \tag{25}$$

$$y_{(n-1)'}=a_3x_{n'}+b_3 \tag{26}$$

Constants in these equations are given as follows.

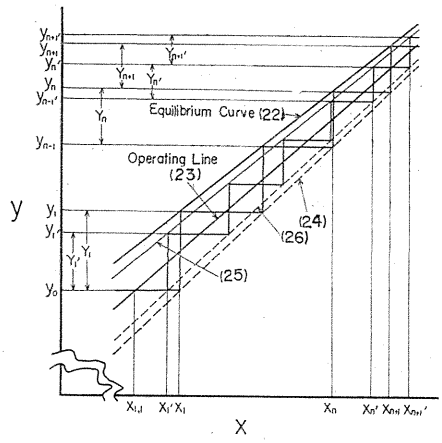

Fig. 11. Stepwise construction for the case when the equilibrium curve is a straight line. Steps drawn between lines (22) and (24) are for ideal plates, and those drawn between lines (25) and (26) are for a constant plate efficiency over the column.

$$a_2=(L/V)[\{2-2(E_{MV})_{1/2}+\lambda(E_{MV})_{1/2}\}/\{2-(E_{MV})_{1/2}\}] \tag{27}$$

$$a_3=(L/V)[\{2-\lambda(E_{MV})_{1/2}\}/\{2-(E_{MV})_{1/2}\}] \tag{28}$$

$$b_2=[2\{1-(E_{MV})_{1/2}\}(D/V)x_D+b_1(E_{MV})_{1/2}]/\{2-(E_{MV})_{1/2}\} \tag{29}$$

$$b_3=\{2(D/V)x_D-b_1(E_{MV})_{1/2}\}/\{2-(E_{MV})_{1/2}\} \tag{30}$$

At $x=x_n$, Y_n shown in Fig. 11 is obtained by subtracting Eq. (24) from Eq. (22).

$$Y_n=y_n-y_{n-1}=2(L/V)(\lambda-1)x_n+2\{b_1-(D/V)x_D\} \tag{31}$$

Also the slope of line (24) can be written as

$$Y_n/(x_{n+1}-x_n)=(L/V)(2-\lambda) \tag{32}$$

From Eqs. (31) and (32), a relation between Y_{n+1} and Y_n is obtained

$$Y_{n+1}=2(L/V)(\lambda-1)x_{n+1}+2\{b_1-(D/V)x_D\}=\{\lambda/(2-\lambda)\}Y_n \tag{33}$$

Thus, the series $\{Y_n\}$ is a geometrical progression and the sum of the series is

$$(SUM)_N=\sum_1^N Y_n=\frac{Y_1(1-r^N)}{1-r}=\frac{Y_1(2-\lambda)(1-r^N)}{2(1-\lambda)} \tag{34}$$

where

$$r=\lambda/(2-\lambda) \tag{35}$$

In the same way, the relation between $Y_{(n+1)'}$ and $Y_{n'}$ shown in Fig. 11 is derived as

$$Y_{(n+1)'}=[\{(\lambda-2)(E_{MV})_{1/2}+2\}/\{2-\lambda(E_{MV})_{1/2}\}]Y_{n'} \tag{36}$$

And the sum of series $\{Y_{n'}\}$ is given by

$$(SUM)_{N'}=\sum_{1'}^{N'} Y_{n'}=\frac{Y_{1'}\{2-\lambda(E_{MV})_{1/2}\}}{(1-\lambda)(E_{MV})_{1/2}}(1-r'^{N'}) \tag{37}$$

where

$$r'=\{(\lambda-2)(E_{MV})_{1/2}+2\}/\{2-\lambda(E_{MV})_{1/2}\} \tag{38}$$

Equating $(SUM)_N$ and $(SUM)_{N'}$

$$\frac{Y_1(2-\lambda)}{2(1-\lambda)}(1-r^N)=\frac{Y_{1'}\{2-\lambda(E_{MV})_{1/2}\}}{2(1-\lambda)(E_{MV})_{1/2}}(1-r'^{N'}) \tag{39}$$

The ratio of Y_1 to $Y_{1'}$ shown in Fig. 11 is

$$\begin{aligned}Y_1/Y_{1'}&=(x_1-x_{1,1})/(x_{1'}-x_{1,1})\\&=\{2-\lambda(E_{MV})_{1/2}\}/\{(2-\lambda)(E_{MV})_{1/2}\}\end{aligned} \tag{40}$$

From Eqs. (39) and (40), the column efficiency E_T which is the ratio of the number of theoretical plates N to that of practical plates N' is given as

$$\begin{aligned}(1/E_T)&=N'/N=(\log r)/(\log r')\\&=\frac{\log\lambda/(2-\lambda)}{\log[\{(\lambda-2)(E_{MV})_{1/2}+2\}/\{2-\lambda(E_{MV})_{1/2}\}]}\end{aligned} \tag{41}$$

For the various values of $(E_{MV})_{1/2}$, the relation between $1/E_T$ and λ is shown in Fig. 12 with solid lines. All the curves pass through a minimum at $\lambda=1$. In Fig, 12,

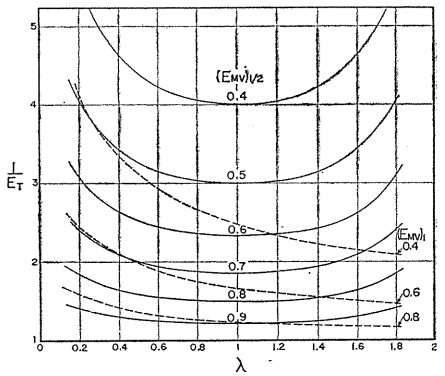

Fig. 12. Relation between $1/E_T$ and λ with $((E_{MV})_{1/2}$ as parameter. Broken lines show Lewis's relation.

broken lines represent Lewis's relation[1] for $(E_{MV})_1$. These curves do not have any minimum and their values decrease with the increase of λ (i. e., the decrease of reflux ratio).

Since the equilibrium curve is usually not a straight line, the value of λ varies with the composion. Therefore, Eq. (41) cannot be used directly, and an average value of λ should be used.

$1/E_T$ obtained by the graphical method as shown in Fig. 13, are plotted against $1/(E_{MV})_{1/2}$ in Fig. 14. In Fig. 14, solid lines show $1/E_T$ calculated by Eg. (41). In this calculation the range of x was divided into two regions where $\lambda>1$ and $\lambda\leqq1$,

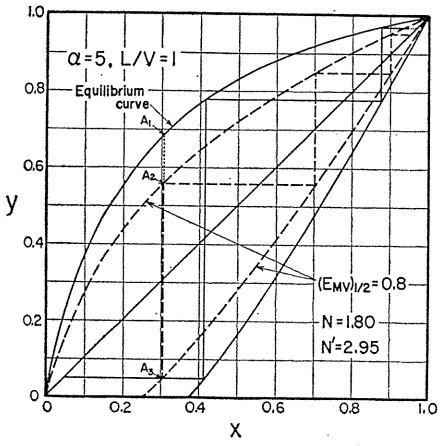

Fig. 13. Stepwise construction to determine number of theoretical plates (solid curves) and the number of practical plates for $(E_{MV})_{1/2}=0.8$ (broken cnrves).

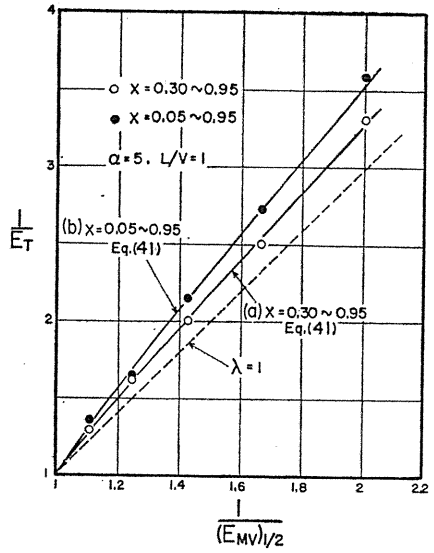

Fig. 14. Comparison of column efficiencies E_T calculated by Eq. (41) and those obtained by the graphical method described in Fig. 13. Broken line represents the values of $1/E_T$ calculated by Eq. (41) at $\lambda=1$. where $1/E_T$ becomes minimum.

and the average values of λ were used for each region. The values by graphical method and by Eq. (41) are in good agreement.

4. 2. Consideration of liquid mixing on the plate

4. 2. 1. Graphical method[12]

In the practical column, liquid on the plate is mixed by bubbling of vapor. Using the eddy diffusion model, the liquid composition on a plate is given by Eq. (10). Therefore, in taking the material balance for the system shown in Fig. 9, the mass transfer rate by eddy diffusion through the boundary at the center of plate must be taken into account, and then the following equation is obtained.

$$\frac{y_{n-1}+y_n}{2}=\left(\frac{L}{V}\right)\left\{x_n-\frac{D_E A\rho_L}{L}\left.\frac{dx}{dz}\right|_{z=Z/2}\right\}+\left(\frac{D}{V}\right)x_D$$

$$=\left(\frac{L}{V}\right)\left(x_n-\frac{1}{N_{Pe}}\left.\frac{dx}{dw}\right|_{w=1/2}\right)+\left(\frac{D}{V}\right)x_D \qquad (42)$$

The composition gradient at the center of plate is given with the derivative of Eq. (10).

$$\left.\frac{dx}{dw}\right|_{w=1/2}=\frac{\eta(\eta+N_{Pe})[1-exp\{\eta+(N_{Pe}/2)\}]}{\eta+(\eta+N_{Pe})exp\{\eta+(N_{Pe}/2)\}}(x_n-x^*_{n-1}) \qquad (43)$$

Substituting Eq. (43) into Eq. (42)

$$(y_{n-1}+y_n)/2=(L/V)[x_n+\{F(N_{Pe},\ \eta)\}(x_n-x^*_{n-1})]+(D/V)x_D \qquad (44)$$

where

$$F(N_{Pe},\ \eta)=\frac{\eta(\eta+N_{Pe})[exp\{\eta+(N_{Pe}/2)\}-1]}{N_{Pe}[\eta+(\eta+N_{Pe})exp\{\eta+(N_{Pe}/2)\}]} \qquad (45)$$

The relation between F and λE_{OG} is shown with parameter N_{Pe} in Fig. 15. For the plug flow of liquid, the value of F is zero. It increases with the increase of mixing

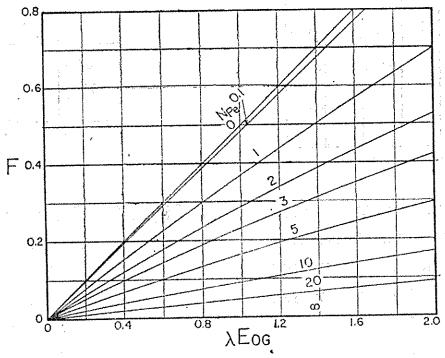

Fig. 15. Relation between F amd λE_{OG} with parameter N_{Pe}.

degree, i. e., the decrease of N_{Pe}, and becomes $\lambda E_{OG}/2$ for the complete mixing of liquid. Values of F are shown in Table 1 for practical cases, and they are between 0.01 and 1.0. Although the value of F varies with λ and N_{Pe}, it is considered to be small in the usual commercial column.

Table 1. Value of F in practical columns

System	Acetone-Benzene[13]	n-Pentane-p-Xylene[13]	Methanol-Toluene[14]	i-Octane-Toluene[20]
E_{OG}	0.702~0.866	0.639~0.843	0.605~0.870	0.553~0.721
λ	0.293~2.58	1.90~10.6	4.10~18.7	0.636~0.764
N_{Pe}	12.0~35.4	9.37~12.32	5.15~7.93	23.7~36.5
F	0.011~0.087	0.116~0.480	0.374~1.00	0.010~0.061

Fig. 16 shows relations of Eqs. (16), (18) and (45) on x-y diagram for the case where the vapor composition from (n-1)th plate is y_{n-1}. When liquid flows as a plug flow ($F=0$), the relation has been shown by the broken line for $N_{Pe}=\infty$, and the liquid composition at the center of n-th plate is given by A_2 as an abscissa of point B_7. When liquid is completely mixed, the liquid composition x_n at the center of plate coincides with the composition $x_{n,1}$ given by A_3 as an absissa of point B_8,

and the relation is shown by the dotted line for $N_{Pe}=0$.

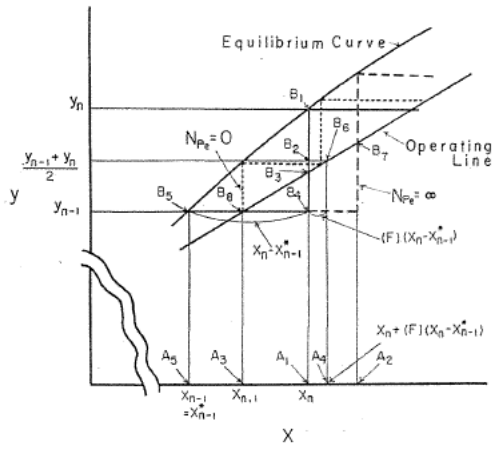

Fig. 16. Stepwise construction when mixing occures on the plate. Dotted line for $N_{Pe}=0$ and broken line for $N_{Pe}=\infty$, represent the case of complete mixing and the plug flow of liquid, respectivelly.

For any degree of liquid mixing on the plate, point B_3 in Fig. 16 lies somewhere between point B_7 and B_8 on the operating line. The vertical line from point B_3 cuts the equilibrium curve at B_1 which gives the composition of vapor leaving n-th plate. Point B_6 is obtained as an intersection of a horizontal line through $(y_{n-1}+y_n)/2$ with the operating line. The abscissa of B_6 is given by Eq. (45) as $x_n+(F)(x_n-x^*_{n-1})$ by point A_4. Here, x^*_{n-1} is the abscissa of B_5 (the point on the equilibrium curve). As the degree of liquid mixing on the plate increases (i. e., N_{Pe} decreases), the value of F showing the distance $\overline{A_1A_4}$ increases, and point B_3 shifts from B_7 towards B_8. Thus, the difference between the liquid compositions at the inlet and oulet of the plate changes with the liquid mixing degree.

In Fig. 16, $\overline{B_1B_4}$ can be expressed as

$$\overline{B_1B_4}=y_n-y_{n-1}=m(x_n-x^*_{n-1}) \tag{46}$$

B_2 is the middle point of $\overline{B_1B_4}$, therefore

$$\overline{B_2B_3}=(1/2)(\overline{B_1B_4})-\overline{B_3B_4}=(m/2)(x_n-x^*_{n-1})-\overline{B_3B_4} \tag{47}$$

Also, in Fig. 16, the slope of operating line is expressed by

$$(\overline{B_2B_3})/\{(F)(x_n-x^*_{n-1})\}=L/V \tag{48}$$

From Eqs. (47) and (48)

$$\overline{B_3B_4}=\{(m/2)-(F)(L/V)\}(x_n-x^*_{n-1}) \tag{49}$$

$\overline{B_1B_4}$, that is, (y_n-y_{n-1}), is divided into two parts by the operating line. The ratio of these parts is given by

$$\frac{\overline{B_3B_4}}{\overline{B_1B_3}}=\frac{\{(m/2)-(F)(L/V)\}(x_n-x^*_{n-1})}{\{(m/2)+(F)(L/V)\}(x_n-x^*_{n-1})}=\frac{\lambda-2F}{\lambda+2F} \tag{50}$$

For the complete mixing of liquid, the value of F becomes $\lambda E_{OG}/2$. Thus, the ratio given by Eq. (50) becomes zero for the ideal plate ($E_{OG}=1$). Then, the stepwise construction shown in Fig. 16 with the dotted line coincides with McCabe-Thiele's method.

When liquid flows as a plug flow, $F=0$, the ratio given by Eq. (50) becomes unity, and the stepwise construction shown in Fig. 16 with the broken line coincides with that described in § 4. 1. 1.

For any degree of liquid mixing, by drawing the locus of point A_3 which satisfies the relation $\overline{A_2A_3}/\overline{A_1A_2}=(\lambda-2F)/(\lambda+2F)$ as shown in Fig. 17, the number of theoretical plates is obtained by the stepwise constion between the locus and the equilibrium curve.

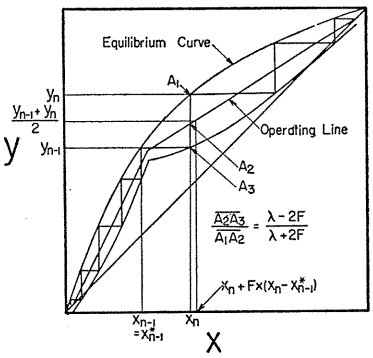

Fig. 17. stepwise construction to calculate the number of plates.

4. 2. 2. *Relation between* $(E_{MV})'_{1/2}$ *and* $(E_{MV})_{1/2}$[12]

In practice, it is difficult to know the liquid composition x_n at the center of plate. Therefore the mean value of inlet and outlet liquid compositions is used instead of x_n in the calculation of plate efficiency $(E_{MV})'_{1/2}$, as described in § 3.

Ths mean value of inlet and outlet liquid composition is represented by $x_n+(F)(x_n-x^*_{n-1})$, as shown in Fig. 18. The difference between this mean composition

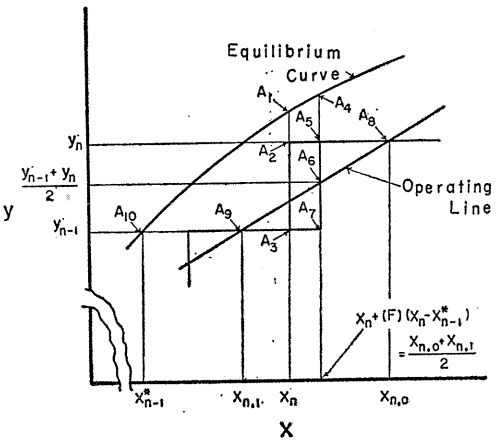

Fig. 18. Rellation between the plate efficiencies $(E_{MV})'_{1/2}$ and $(E_{MV})_{1/2}$.

and the one at the center of plate is given by $(F)(x_n-x^*_{n-1})$. Thus, the following relation between $(E_{MV})'_{1/2}$ and $(E_{MV})_{1/2}$ has been derived from Fig. 18 as follows.

$$\frac{(E_{MV})_{1/2}}{(E_{MV})'_{1/2}}=\frac{(\overline{A_2A_3})/(\overline{A_1A_3})}{(\overline{A_5A_7})/(\overline{A_4A_7})}=\frac{\overline{A_4A_7}}{\overline{A_1A_3}}=\frac{\overline{A_{10}A_7}}{\overline{A_{10}A_3}}$$

$$=\frac{\{x_n+(F)(x_n-x^*_{n-1})\}-x^*_{n-1}}{x_n-x^*_{n-1}}=1+F \qquad (51)$$

This relation is shown in Fig. 19. For $\lambda E_{OG}<1$, the difference between $(E_{MV})'_{1/2}$

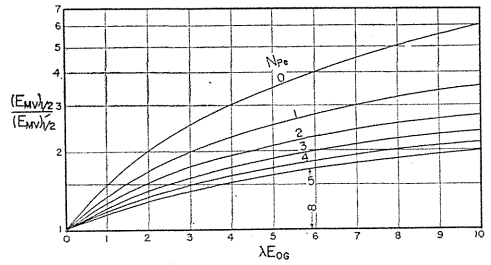

Fig. 19. Ratio of plate efficiencies $(E_{MV})_{1/2}$ to $(E_{MV})'_{1/2}$ given by Eq. (51).

and $(E_{MV})_{1/2}$ is 50% at the maximum for the complete mixing of liquid, and the difference is smaller for the larger diameter of column, because the diameter becomes large then the value of N_{Pe} becomes large.

4. 2. 3. Relation between column efficiency and plate efficiency[25]

Under the assumptions that the equilibrium curve is a straight line and the plate efficiency is constant over the column, a relation between the column efficiency E_T and the plate efficiency $(E_{MV})_{1/2}$ is derived as follows.

The equilibrium and operating lines are given by Eqs. (22) and (23) respectively, and these are shown in Fig. 20 on x-y diagram. Using the notations given in Fig. 20, the following relations are obtained from the definition of the plate efficiency and the slope of equilibrium line.

$$\overline{A_2A_5}=y_{n'}-y_{(n-1)'}=(E_{MV})_{1/2}(\overline{A_1A_5})$$
$$=m(E_{MV})_{1/2}(x_{n'}-x^*_{(n-1)'}) \qquad (52)$$
$$\overline{A_3A_4}=(\overline{A_2A_5})/2-\overline{A_4A_5}$$
$$=(m/2)(E_{MV})_{1/2}(x_{n'}-x^*_{(n-1)'})-\overline{A_4A_5} \qquad (53)$$

The slope of operating line is given by

$$\frac{L}{V}=\frac{\overline{A_3A_4}}{\overline{A_3A_6}}=\frac{\overline{A_3A_4}}{(F)(x_{n'}-x^*_{(n-1)'})} \qquad (54)$$

Eq. (53) is substituted into Eq. (54), and rearranged to

$$\overline{A_4A_5}=\{(m/2)(E_{MV})_{1/2}$$
$$-(F)(L/V)\}(x_{n'}-x^*_{(n-1)'}) \qquad (55)$$

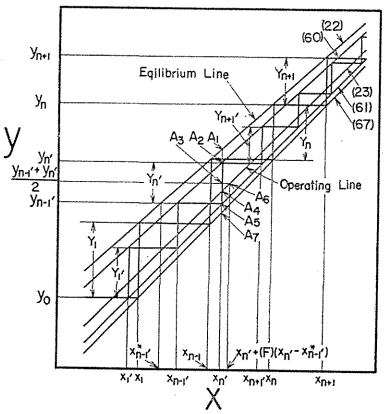

Fig. 20. Illustration for determine the number of theoretical and practical plates.

From Eqs. (52) and (55)

$$(\overline{A_4A_5})/(\overline{A_2A_4}) = (\overline{A_4A_5})/(\overline{A_2A_5}-\overline{A_4A_5})$$
$$= \{\lambda(E_{MV})_{1/2}-2F\}/\{\lambda(E_{MV})_{1/2}+2F\} \tag{56}$$

Thus, in Fig. 20, $\overline{A_2A_5}$, i. e., the variation of vapor composition between the plates $(y_{n'}-y_{(n-1)'})$, is divided by the operating line so as to satisfy Eq. (56).

In Fig. 20, the plate efficiency is expressed as follows.

$$(E_{MV})_{1/2} = (\overline{A_2A_5})/(\overline{A_1A_5}) = (\overline{A_2A_4}+\overline{A_4A_5})/(\overline{A_1A_4}+\overline{A_4A_5}) \tag{57}$$

From Eqs. (56) and (57), following relations are derived.

$$(\overline{A_2A_4})/(\overline{A_1A_4}) = \{\lambda(E_{MV})_{1/2}+2F\}/[\lambda\{2-(E_{MV})_{1/2}\}+2F] \tag{58}$$

$$(\overline{A_4A_5})/(\overline{A_1A_4}) = \{\lambda(E_{MV})_{1/2}-2F\}/[\lambda\{2-(E_{MV})_{1/2}\}+2F] \tag{59}$$

Under the assumption that $(E_{MV})_{1/2}$ is constant over the column, the loci of points A_2 and A_5, which satisfy Eqs. (58) and (59) for any value of x, are drawn in Fig. 20. These loci are exbressed by

$$y_{n'} = a_3x_{n'}+b_3 \tag{60}$$

$$y_{(n-1)'} = a_4x_{n'}+b_4 \tag{61}$$

The constants in Eqs. (60) and (61) are determined as follows.

$$\frac{a_3-(L/V)}{m-(L/V)} = \frac{b_3-(D/V)x_D}{b_1-(D/V)x_D} = \frac{\lambda(E_{MV})_{1/2}+2F}{\lambda\{2-(E_{MV})_{1/2}\}+2F} \tag{62}$$

$$a_3 = (L/V)\lambda\{2-(2-\lambda)(E_{MV})_{1/2}+2F\}/[\lambda\{2-(E_{MV})_{1/2}\}+2F] \tag{63}$$

$$b_3 = \frac{\lambda[2\{1-(E_{MV})_{1/2}\}(D/V)x_D+b_1(E_{MV})_{1/2}]+2b_1F}{\lambda\{2-(E_{MV})_{1/2}\}+2F} \tag{64}$$

Similarly,

$$a_4 = (L/V)\lambda\{2-\lambda(E_{MV})_{1/2}+2F\}/[\lambda\{2-(E_{MV})_{1/2}\}+2F] \tag{65}$$

$$b_4 = [\lambda\{2(D/V)x_D-b_1(E_{MV})_{1/2}\}+2b_1F]/[\lambda\{2-(E_{MV})_{1/2}\}+2F] \tag{66}$$

For ideal plates, Eq. (61) is rewritten as:

$$y_{n-1} = a_2x_n+b_2 \tag{67}$$

where

$$a_2 = (L/V)\lambda\{2-\lambda+2(F)_{E_{OG}=1}\}/\{\lambda+2(F)_{E_{OG}=1}\} \tag{68}$$

$$b_2 = [\lambda\{2(D/V)x_D-b_1\}+2b_1(F)_{E_{OG}=1}]/\{\lambda+2(F)_{E_{OG}=1}\} \tag{69}$$

The number of theoretical plates is determined by the stepwise construction between lines (22) and (67) in Fig. 20, and the relation between Y_n and Y_{n+1} is derived with the same way as the derivation of Eq. (33), as follows.

$$Y_{n+1}=(m-a_2)\{(Y_n/a_2)+x_n\}+(b_1-b_2)=(m/a_2)Y_n \tag{70}$$

Thus, the series $\{Y_n\}$ is a geometrical progression, and the sum of the series is

$$(SUM)_N=\sum_1^N Y_n=\frac{Y_1(1-r^N)}{1-r} \tag{71}$$

where

$$r=(m/a_2)=\{\lambda+2(F)_{E_{OG}=1}\}/\{2-\lambda+2(F)_{E_{OG}=1}\} \tag{72}$$

On the other hand, the number of practical plates is determined by the stepwise construction between lines (60) and (61), as shown in Fig. 20. In the same way as for Y_n, the relation between $Y_{n'}$ and $Y_{(n+1)'}$ is derived.

$$Y_{(n+1)'}=(a_3/a_4)Y_{n'} \tag{73}$$

The sum of geometrical series $\{Y_{n'}\}$ is

$$(SUM)_{N'}=\sum_1^N Y_{n'}=\frac{Y_{1'}(1-r'^{N'})}{1-r'} \tag{74}$$

where

$$r'=a_3/a_4=\{2-(2-\lambda)(E_{MV})_{1/2}+2F\}/\{2-\lambda(E_{MV})_{1/2}+2F\} \tag{75}$$

The starting point of stepwise constructions for both the theoretical and practical cases is chosen as y_0, and Y_1 and $Y_{1'}$ are given by the following relations as shown in Fig. 20.

$$\begin{aligned}Y_1&=(m-a_2)(y_0-b_2)/a_2+(b_1-b_2)\\&=2\{(\lambda-1)y_0+b_1-\lambda(D/V)x_D\}/\{2-\lambda+2(F)_{E_{OG}=1}\}\end{aligned} \tag{76}$$

$$Y_{1'}=2(E_{MV})_{1/2}\{(\lambda-1)y_0-b_1-\lambda(D/V)x_D\}/\{2-\lambda(E_{MV})_{1/2}+2F\} \tag{77}$$

After equating $(SUM)_N$ and $(SUM)_{N'}$ and from Eqs. (71) ~ (77), the following expression is obtained.

$$r^N=r'^{N'} \tag{78}$$

The column effiency E_T is given by the following relation.

$$\begin{aligned}1/E_T&=N'/N=(\log r)/(\log r')\\&=\left[\log\frac{\lambda+2(F)_{E_{OG}=1}}{2-\lambda+2(F)_{E_{OG}=1}}\right]/\left[\log\frac{2-(2-\lambda)(E_{MV})_{1/2}+2F}{2-\lambda(E_{MV})_{1/2}+2F}\right]\end{aligned} \tag{79}$$

From Eq. (79) the column efficiency can be calculated for any degree of liquid mixing on the plate. For the plug flow of liquid, $F=0$, Eq. (79) coincides with Eq. (41). On the other hand, for the complete mixing of liquid,

$$F=\lambda E_{OG}/2=\lambda(E_{MV})_{1/2}/2=\lambda(E_{MV})_1/2 \tag{80}$$

Eq. (79) coincides with Lewis's relation as follows.

$$1/E_T=(\log\lambda)/[\log\{1-(E_{MV})_{1/2}+\lambda(E_{MV})_{1/2}\}]$$
$$=(\log\lambda)/[\log\{1-(E_{MV})_1+\lambda(E_{MV})_1\}] \quad (81)$$

For $(E_{MV})_{1/2}=0.5$, $1/E_T$ calculated by Eq. (79) are shown with parameter N_{Pe} in Fig. 21. Although $1/E_T$ shows minimum at $\lambda=1$ for the plug flow of liquid ($N_{Pe}=\infty$), with the decrease of N_{Pe} the minimum point shifts to the right hand side, i. e., larger value of λ. Fig. 21 shows that $1/E_T$ decrases with the increase of mixing degree, and it seems that for a constant value of $(E_{MV})_{1/2}$ the higher the mixing degree, the smaller the number of practical plates. However, the number of theoretical plates varies also with the liquid mixing degree, and the dependence of the number of practical plates on the mixing degree cannot be determined from $1/E_T$ only. For example, in the case of $\lambda=1$ in Fig. 21, $1/E_T$ for the complete mixing is 2/3 times that for the plug flow of liquid. The number of theoretical plates for the complete mixing is twice as large as that for the plug flow. As the result, the number of practical plates for the complete mixing of liquid is larger by 4/3 times than that for the plug flow of liquid. In general, it can be concluded that the number of practical plates to separate the mixture into desired products increases with the mixing degree of liquid.

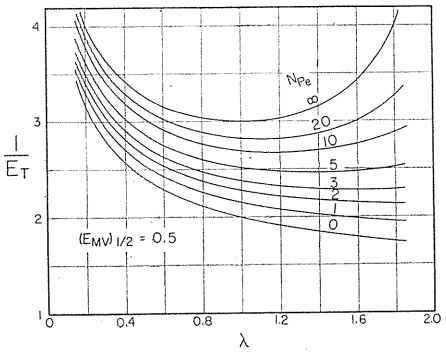

Fig. 21. Values of $1/E_T$ calculated by Eq. (79) with parameter N_{Pe} for $(E_{MV})_{1/2}=0.5$.

Eq. (79) has been derived unber the assumption that the equilibrium curve is a straight line. However, as the equilibrium curve is usually not straight, the average value of λ should be used in the calculation of Eq. (79).

The numbers of theoretical and practical plates are determined by the graphical method as shown in Fig. 22. In this figrue, curve (67)′ is drawn so as to satisfy the following relation,

$$\frac{(\overline{A_4A_7})}{(\overline{A_1A_4})}=\frac{\{\lambda-2(F)_{E_{OG}=1}\}}{\{\lambda+2(F)_{E_{OG}=1}\}} \quad (82)$$

and curves (60)′ and (61)′ are drawn in accordance with Eqs. (58) and (59). $1/E_T$ obtained by the graphical method are plotted in Fig. 23. The solid lines show the results calculated by Eq. (79), and coincide with the results by graphical method satisfactorily. Thus, Eq. (79) can be used with the average value of λ when the equilibrium curve is not a straignt line.

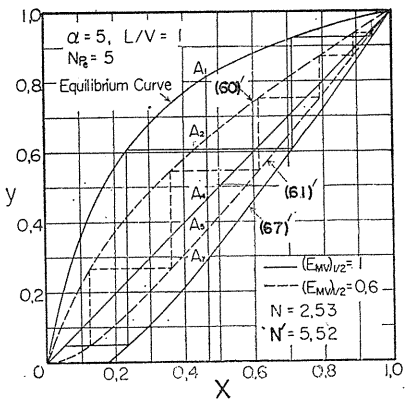

Fig. 22. Stepwise construction to determine the number of theoretical and practical plates.

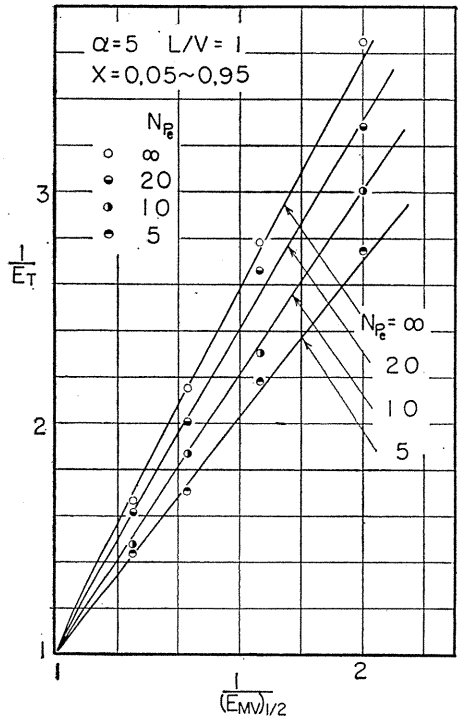

Fig. 23. Comparison of $1/E_T$ calculated by Eq. (79) (solid lines) and those obtained by the graphical method (points).

4. 2. 4. Relation between $(E_{ML})_{1/2}$ *and* $(E_{MV})_{1/2}$[25]

Although the plate efficiency based on the vapor composition, $(E_{MV})_{1/2}$, is logical, the plate efficiency, $(E_{ML})_{1/2}$ based on the liquid composition is often used in industry. The relation between the plate efficiencies $(E_{ML})_{1/2}$ and $(E_{MV})_{1/2}$ is derived as follows. The slope of curve (61)′ shown in Fig. 24 is given by Eq. (65) as

$$a_4=\frac{y_n-y_{n-1}}{x_{n+1}-x_n}$$

$$=\left(\frac{L}{V}\right)\frac{\lambda\{2-\lambda(E_{MV})_{1/2}+2F\}}{\lambda\{2-(E_{MV})_{1/2}\}+2F} \quad (83)$$

And the slope of equilibrium curve and $(E_{MV})_{1/2}$ are expressed, respectively, as follows.

$$m=(y_n^*-y_n)/(x_n-x_n^*) \quad (84)$$

$$(E_{MV})_{1/2}=(y_n-y_{n-1})/(y_n^*-y_{n-1}) \quad (85)$$

From Eqs. (83), (84) and (85), the plate efficiency $(E_{ML})_{1/2}$ based on the liquid co-

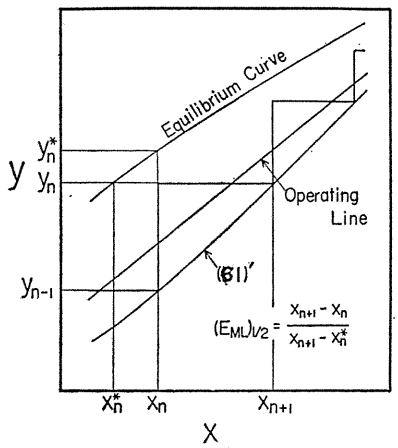

Fig. 24. Diagram to illustrate the plate efficiency $(E_{ML})_{1/2}$ based on liquid at the canter of the plate.

mposition is derived as a function of $(E_{MV})_{1/2}$, λ and F.

$$(E_{ML})_{1/2}=(x_{n+1}-x_n)/(x_{n+1}-x_n^*)$$
$$=\frac{(E_{MV})_{1/2}\{2\lambda-\lambda(E_{MV})_{1/2}+2F\}}{(\lambda-2)(E_{MV})_{1/2}+2(1+F)} \tag{86}$$

When liquid on the plate flows as a plug flow, $F=0$, Eq. (86) becomes as follows.

$$(E_{ML})_{1/2}=\lambda(E_{MV})_{1/2}\{2-(E_{MV})_{1/2}\}/\{\lambda-2)(E_{MV})_{1/2}+2\} \tag{87}$$

On the other hand, when liquid on the plate is completely mixed, $F=\lambda(E_{MV})_{1/2}/2$. As a result, Eq. (86) is rearranged as follows.

$$(E_{ML})_{1/2}=(E_{MV})_{1/2}/[(E_{MV})_{1/2}+(1/\lambda)\{1-(E_{MV})_{1/2}\}] \tag{88}$$

Eq. (88) is the same relation as that derived for Murphree's plate efficiencies $(E_{MV})_1$ and $(E_{ML})_1$, which are based on the vapor and liquid composions respectively.

4. 3. *Calculation for multicomponent system*[26]

4. 3. 1. *Graphical method for ternary system*

For a binary system the number of theoretical plates can be determined easily by the graphical method as shown in Fig. 17. However, the same locus as that of point A_3 in Fig. 17 can not be drawn beforehand for the system containing more than three components.

For a ternary system a graphical method starting from the top of the column can be applied. An example is shown in Fig. 25 for benzene-toluene-xylene system.

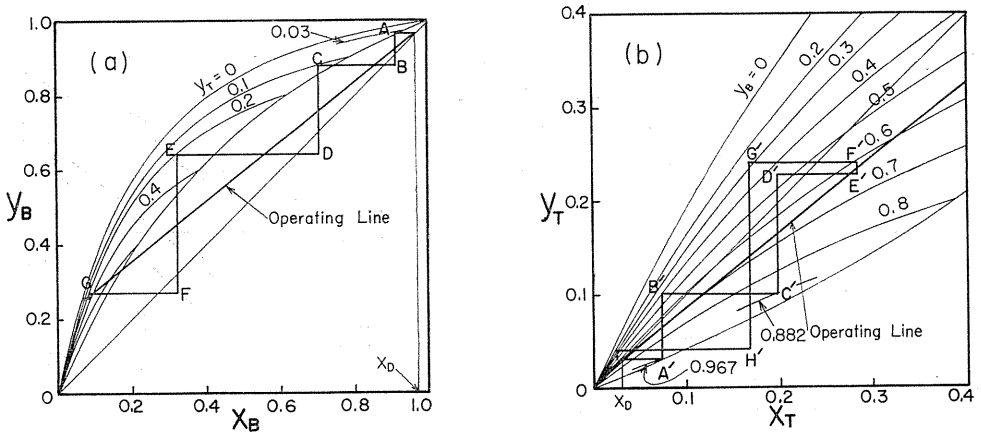

Fig. 25. Stepwise construction for benzene-toluene-m-xylene system.

Fig. 25-a is x-y diagram for benzene, and the equilibrium curves are drawn with the vapor compositions of toluene as parameters. Fig. 25-b is that for toluene, and the paramers are the vapor compositions of benzene. In Fig. 25-a, a horizontal line $y_B=x_{B,D}$ intersects the equilibrium curve $y_T=x_{T,D}$ at point A, and the liquid com-

position $x_{B,t}$ on the top plate is given as an abscissa of point A. A point B is determined by Eq. (50) with the same way as for binary system (in this examle F=0), and $y_{B,t-1}$ is given as an ordinate of point B. In the same way, point A′ and B′ are located in Fig. 25-b, and $x_{T,t}$ and $y_{T,t-1}$ are determined. Furthermore, point C′ is obtained as an intersection point of $y_T=y_{T,t-1}$ and equilibrium curve $y_B=y_{B,t-1}$, and D′ is located so as to satisfy Eq. (50). From these points, $x_{T,t-1}$ and $y_{T,t-2}$ are determined. Returning to Fig. 25-a, point C, D, E and F are determined with the same way as described above. Similarly, repeating this procedure, the compositions on the lower plate are determined successively.

For the ternary system, it is possible to apply the graphical method starting from the top condition, but it is difficult to do it from the bottom condition. This graphical method can not be applied for the system containing more than four components, and moreover the method is troublesome in drawing the equilibriumn curves.

4. 3. 2. Step-to-step calculation

Eq. (44) is rewritten by substituting $x_{i,n}-x^*_{i,n-1}=(y_{i,n}-y_{i,n-1})/m$ as follows.

$$(y_{i,n-1}+p_iy_{i,n})/(1+p_i)=(L/V)x_{i,n}+(D/V)x_D \tag{89}$$

where p_i is the ratio given by Eq. (50), and written as

$$p_i=(\lambda-2F_i)/(\lambda+2F_i) \tag{90}$$

The step-to-step calculation from the top of column is carried out as follows. The vapor composition of top plate is given as $y_{i,t}=x_{i,D}$, and the liquid composition $x_{i,t}$ is determined as a value in equilibrium with $y_{i,t}$. For (t-1)th plate, $y_{i,t-1}$ is calculated by Eq. (89), and $x_{i,t-1}$ is obtained as an equilibrium value of $y_{i,t-1}$. Repeating this procedure toward the bottom of column, the number of theoretical plates is determined.

On the other hand, the step-to-step calculation starting from the bottom of column is given as follows. For the stripping section, the following equation is derived in the same way as the derivation of Eq. (89).

$$(y_{i,n-1}+p_iy_{i,n})/(1+p_i)=(L'/V')x_{i,n}-(W/V')x_{i,w} \tag{91}$$

Definig a modified relative volatility of i-component on n-th plate as follows,

$$\alpha'_{i,n}=\{y_{i,n}(1-x_{i,n})\}/\{x_{i,n}(1-y_{i,n})\} \tag{92}$$

the vapor composition can be written with the same equation as for a binary system.

$$y_{i,n}=\alpha'_{i,n}x_{i,n}/\{1+(\alpha'_{i,n}-1)x_{i,n}\} \tag{93}$$

Eq. (93) is substituted into Eq. (91), and rearranged as follows.

$$ax^2_{i,n}+bx_{i,n}-c=0 \tag{94}$$

where

$$a=(L'/V')(1+p_i)(\alpha'_{i,n}-1) \tag{95}$$

$$b=(L'/V')(1+p_i)-c(\alpha'_{i,n}-1)-p_i\alpha'_{i,n} \tag{96}$$

$$c=y_{i,\,n-1}+(W/V')(1+p_i)x_{i,\,w} \tag{97}$$

$x_{i,\,n}$ is obtained by solving Eq. (94).

$$x_{i,\,n}=(-b+\sqrt{b^2+4ac})/2a \tag{98}$$

On starting the calculation, the bottom composition of liquid is given as $x_{i,\,0}=x_{i,\,w}$, and $y_{i,\,0}$ is obtained as an equilibrium value of $x_{i,\,0}$. To determine $x_{i,\,1}$, Eq. (98) is used. However, Eq. (98) involves an unknown value of $\alpha'_{i,\,n}$ (i. e., $\alpha'_{i,\,1}$). So, instead of $\alpha'_{i,\,1}$, $\alpha'_{i,\,0}$ is used as a first approximation. $x_{i,\,1}$ obtained from Eq. (98) is corrected to be $\Sigma x_{i,\,1}=1$, and $y_{i,\,1}$ is determined as in equilibrium with $x_{i,\,1}$. $\alpha'_{i,\,1}$ calculated by Eq. (92) with $x_{i,\,1}$ and $y_{i,\,1}$ obtained above is used as a second approximation. Repeating this procedure, one can obtaine the right values of $x_{i,\,1}$ and $y_{i,\,1}$. By this repeated calculation, the compositions on each plate are determined successively from the bottom toward the top of the column.

For the calculation of the number of practical plates, the vapor composition on the plate is given by $y_{i,\,n}=(y^*_{i,\,n}-y_{i,\,n-1})(E_{MV})_{1/2}+y_{i,\,n-1}$ and the following equation is used instead of Eq. (90).

$$p_i=\{\lambda(E_{MV})_{1/2}-2F_i\}/\{\lambda(E_{MV})_{1/2}+2F_i\} \tag{99}$$

When the calculation is carried out from the top of column, the liquid composition on the plate is given by $x_{i,\,n}=x_{i,\,n+1}-(x_{i,\,n+1}-x^*_{i,\,n})(E_{ML})_{1/2}$, where $(E_{ML})_{1/2}$ is converted from $(E_{MV})_{1/2}$ by Eq. (86).

4. 3. 3. Effect of liquid mixing on number of plates

The step-to-step calculation was carried out by starting with the bottom condition given in Table 2. As the result, the loci of liquid compositions are shown in Fig. 26 for various mixing degrees of liquid (i. e., N_{Pe}) with $E_{OG}=1$. For the larger value of N_{Pe}, the composition tends to vary at the lower plate number. As the plate number becomes large, the loci for various values of N_{Pe} show the tendency to converge at a point of a definite

Table 2. Conditions for calculation

i	α	x_w
1	1.0	0.70
2	1.5	0.20
3	2.0	0.09
4	3.0	0.01

$L'/V'=1.4$

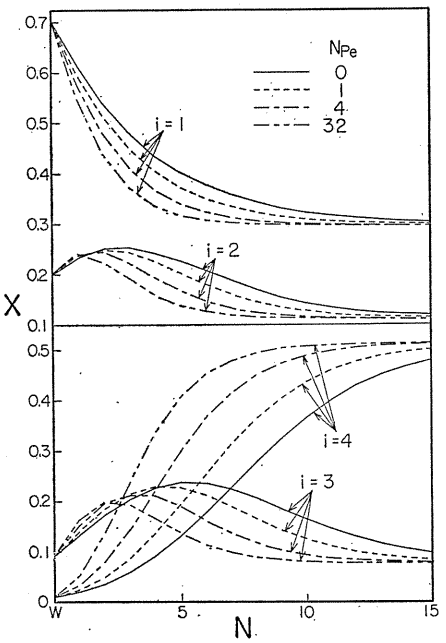

Fig. 26. Loci of liquid composition in the distillation for various mixing degrees of liquid on the plate.

composition. Fig. 27 show the variation of the number of plates with N_{Pe}, in which the ratio of liquid compositions x_1/x_4 varies from 70 to 0.62. The number of plates is maximum for $N_{Pe}=0$ (i. e., the complete mixing of liquid), and it rapidly decreases with the increase of N_{Pe} for $N_{Pe}<10$.

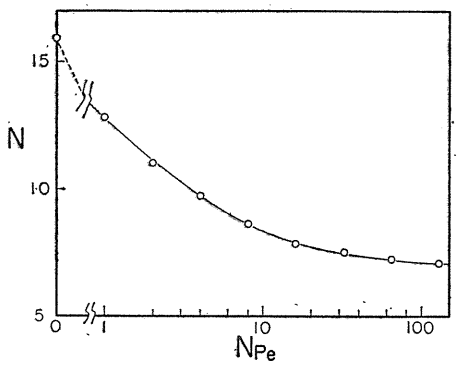

Fig. 27. Variation of number of plates with mixing degrees of liquid on the plate. The range of liquid composition is $x_1/x_4=$ 70~0.62.

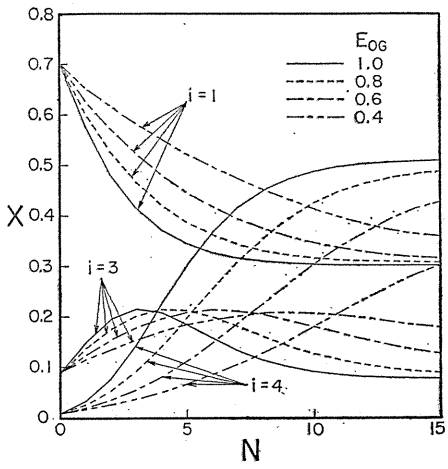

Fig. 28. Loci of liquid composition in the distillation colnmn for various values of the point efficiency.

Fig. 28 shows the loci of liquid composition for various values of point efficiency with $N_{Pe}=4$. These loci do not converge to one point unlike the binary system even if the number of plates become large.

Chapter 5. Eddy diffusivity in liquid on plate

Although Murphree's plate efficiency varies largely with the mixing degree of liquid on the plate, $(E_{MV})_{1/2}$ defined by Eq. (1) is not affected so much by the liquid mixing as described in § 2. However, under the assumption of ideal plate which is used in the definition of $(E_{MV})_{1/2}$, the number of theoretical plates varies considerably with the mixing degree of liquid. Therefore, the eddy diffusivity in liquid plays an important role in the design of the distillation column.

The eddy diffusivities on the sieve plates have been measured by many investigators[27~30]. However, even the bubblecap plate which is used for a long time, the measurements were performed only by Delaware Univ.[13] and Gilbert[31], and the results of these measurements differ largely with one another.

In our laboratry[32, 33], the eddy diffusivities in liquid on the bubble-cap plate were measured, and the effects of operating variables, design variables and physical properties on the eddy diffusivity have been investingated.

5. 1. Experiments

A rectangular column consisted of three plates with bubble-caps was used in

this experiment. Details on the plate and column are given in Table 3. To investigate the effects of operating and design variables on the eddy diffusivity, the

Table 3. Design detais of plates

	Plate 1	Plate 2	Plae 3
Weir length [m]	0.355	0.355	0.249
Z [m]	0.75	0.75	0.315
Bubble caps			
Diameter [m]	0.05	0.077	0.05
Height [m]	0.05	0.06	0.05
Number per plate	36	21	9
Number of caps raws	9	7	3
Layout [m]	P 0.09 triangular arrangement	P 0.115 triangular arrangement	P 0.09 square arrangement
Cap slots			
Height [m]	0.025	0.025	0.025
Width at top [m]	0.04	0.04	0.04
at bottom [m]	0.06	0.06	0.06
Number per cap	18	24	18

steady-state tracer experiments which is the same method as used in Delaware Univ.[13] were carried out for the air-water system by Plate 1 and 2 given in Table 3. An aqueous solution of NaCl was used as a tracer, and the concentration of NaCl was measured by mean of an electric conductivity cell.

The steady-state experiment required a large quantity of liquid. On the other hand, in an unsteady-state technique liquid was pooled on the plate. The latter was used for air-aqueous glycerine solution and air-aqueous methanol solution systems. In this case, Plate 3 was used for the smaller column than that used in the steady-state method. Then a partition weir was set up at the distance of 0.015 m from one side wall, and the tracer was poured into the opening between the side wall and the weir. The weir was removed in a moment, and the salt concentration at a point apart 0.22 m from the side wall mentioned above was measured continuously. From the curve of concentration vs. time on the recording chart paper, the eddy diffusivity was detemined in the same manner as Barker-Self[28].

5. 2. *Effects of operating and design variables on eddy diffusivity*

The eddy diffusivities obtained from steady-state experiments are compared with the values estimated by Delaware's method[13] in Fig. 29. For the large weir height the experimental values agree approximately with the estimated ones. However, for the small weir height the formers are much larger than the latters. The experimental values obtained by Gilbert[31] are also shown in Fig. 29, and these are considerably larger than the estimated ones. Therefore, this estimation method can not be used universally.

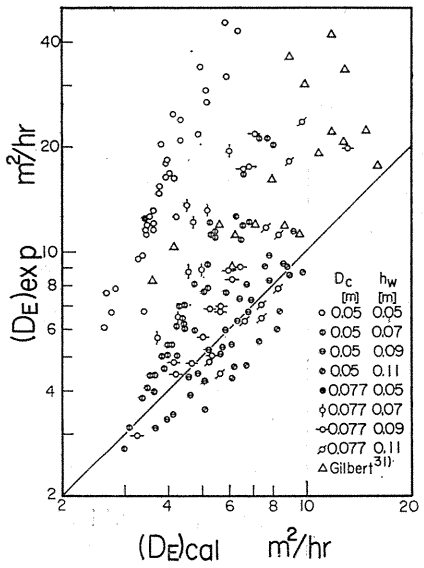

Fig. 29. Comparison of the experimental eddy diffusivities with the values estimated by Delaware's method.

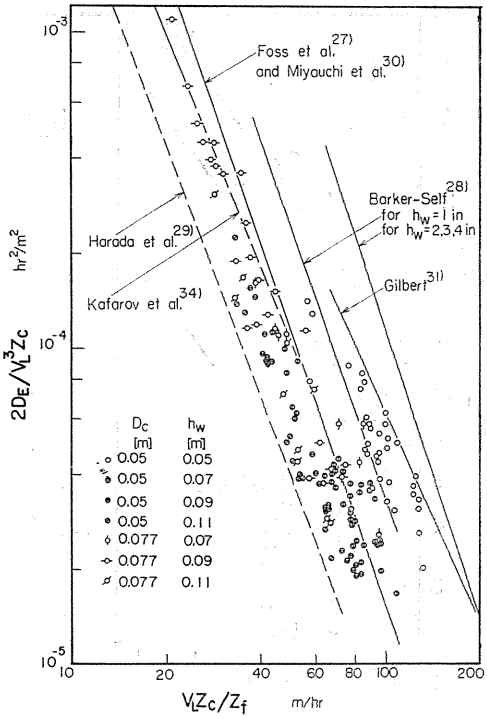

Fig. 30. Comparison of the eddy diffusivities obtained by various investigator.

In Fig. 30, the experimental results are plotted by the correlation method given by Foss et al.[27]. The various correlation lines are also shown in Fig. 30. Except for Gilbert's one, all of these were obtained for sieve plates. The results of our experiment for $h_w=0.05$m are close to Gilbert's line. However, as the weir height becomes large, the data shift toward left on Fig. 30. Almost all data except $h_w=$ 0.05m locate between the line given by Foss *et al.* and the line extrapolated by correlating the data of Harada *et al.*[29].

The eddy diffusivity increases with the gas velocity as shown in Fig. 31. The slope of lines drawn in Fig. 31 decreases with the increase of weir height. When $h_w>0.09$m, the lines turn up for $u>3000$m/hr. This fact comes from the transition of the structure of froth layer for the large weir height. As mentioned by Goederen[35], for the low gas velocity the gas bubbles disperse in the continuous liquid-phase, while for the high gas velocity the liquid sprays disperse in the continuous gas-phase. When Plate 2 (cap diameter=0.077m) was used, the transition occured at about $u=2500$m/hr.

Fig. 32 shows that D_E increases with the liquid flow rate, and the slope of lines drawn in this figure decreses with increase of weir height. D_E for 0.077m cap diameter are larger than those for $D_C=0.05$m as shown in Fig. 33. The same tendency is given in Delaware's report on which D_E for $D_C=6.5$ inch are larger 1.33 times than those for $D_C=3$ inch.

For these results the following correlation has been derived.

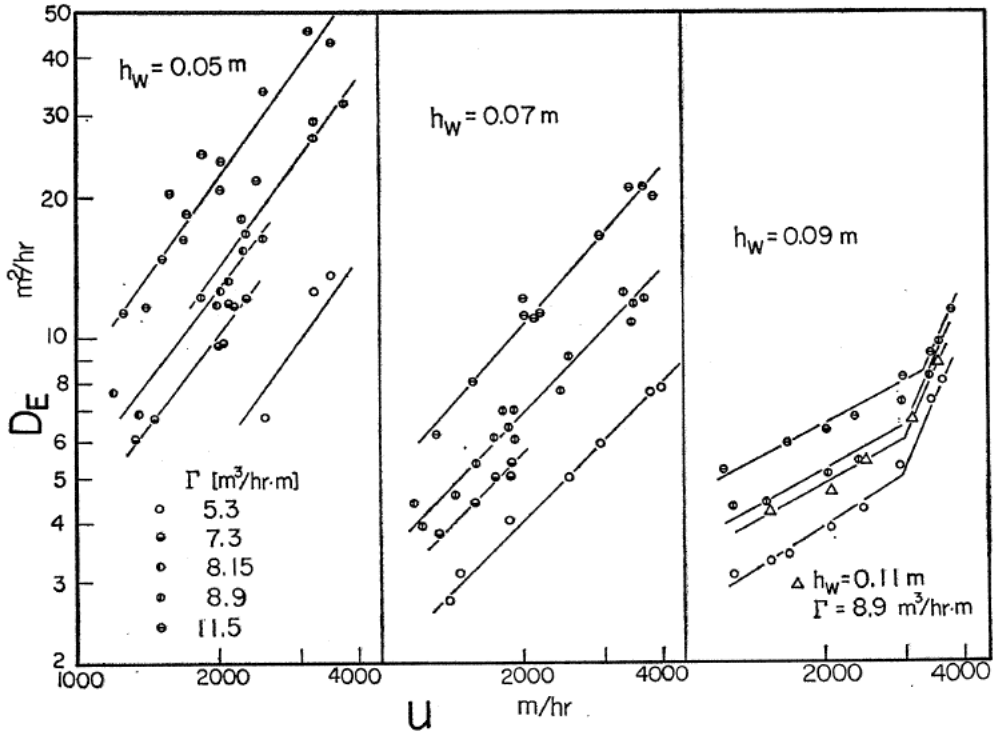

Fig. 31. Effects of the gas velocity on the eddy diffusivity for D_C=0.05m.

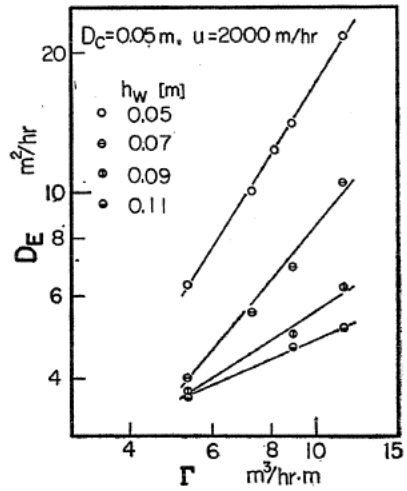

Fig. 32. Effects of the liguid flow rate on the eddy diffusivity.

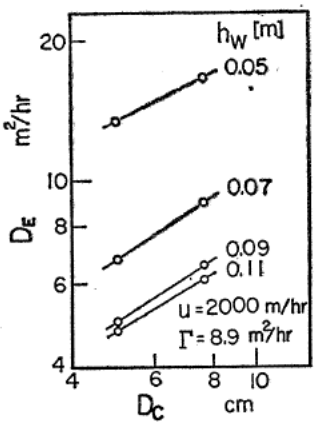

Fig. 33. Effects of the bubble cap diameter on the eddy diffusivity.

$$D_E = 7.29\left(\frac{u}{2000}\right)^{1.89-11.6h_w}\left(\frac{\Gamma}{10}\right)^{2.66-22h_w}(100h_w-4)^{-0.66} \times (100D_C)^{0.53} \qquad (100)$$

where u is the superficial gas velocity [m/hr], Γ the liquid flow rate per unit width [m³/hr·m] and D_C the cap diameter [m]. Eq. (100) was obtained with the following ranges of variables ; $u=1000\sim4000$ m/hr, $\Gamma=5\sim12$ m³/hr·m and $D_C=0.05\sim0.077$ m. The data of the liquid spray region for $h_w>0.09$m and high gas velocity were not used in this correlation. In Fig. 34, the experimental and literature values of D_E are compared with those calculated by Eq. (100), and the standard deviation is 10.8%.

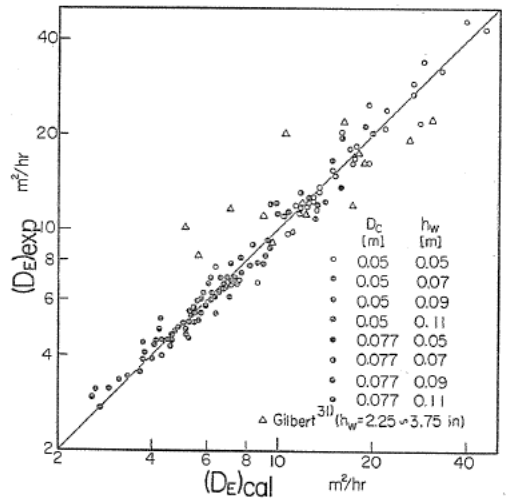

Fig. 34. Comparison of the experimental eddy diffusivities with the values calculated by Eq. (100).

5. 3. *Effect of physical properties on eddy diffusivity*

Almost all measurements concerning the eddy diffusivity on the plate have been carried out for air-water system. Only a few data for other systems appeared in Delaware's report.

For air-aqueous glycerine solution, D_E decreses with the increase of liquid concentration as shown in Fig. 35. As the results, D_E were plotted against the liquid viscosity in Fig. 36, and the effect of viscosity on D_E is given as follows.

$$D_E \propto (\mu/\mu_w)^{-0.21} \qquad (101)$$

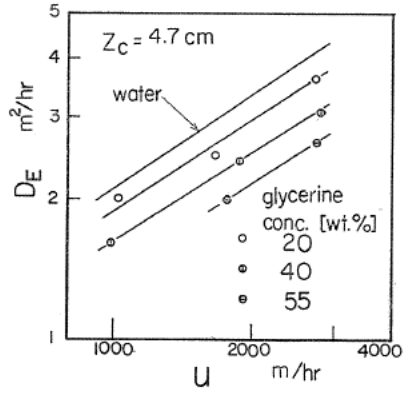

Fig. 35. Eddy diffusivities for air-aqueous glycerine solution system.

where μ_w is the viscosity of water. The decrease of D_E with μ is much larger than the results in Delaware's report where D_E for the aqueous solution of CMC (μ=10 c.p.) is smaller only 6% than that for water.

The eddy diffusivities for air-aqueous MeOH solution are shown in Fig. 37. Although D_E decreases with the increase of MeOH for lower concentration than 1 wt %, for high concentration it does not vary

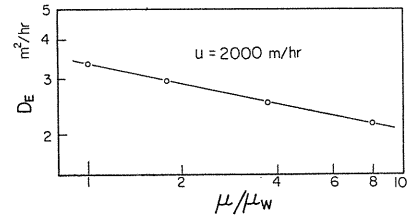

Fig. 36. Effect of liquid viscosity on the eddy diffusivity for air-aqueous glycerine solution system.

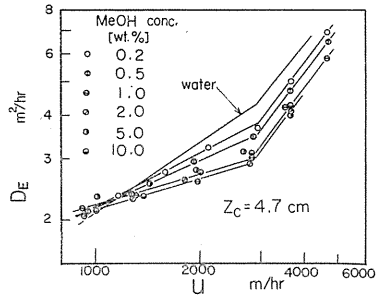

Fig. 37. Eddy diffusivities for air-aqueous MeOH solution system.

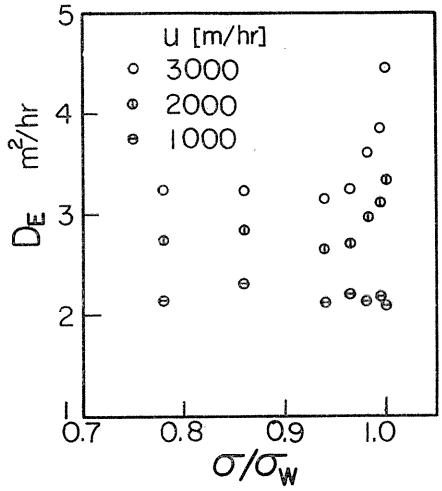

Fig. 38. Effects of surface tension on the eddy diffusivity for air-aqueous MeOH solution system.

with the concentration. For u<3000 m/hr the dependency of D_E on u varies with MeOH concentration. This effect is similar to that of weir height on the dependency of D_E on u in the steady-state experiment for air-water system. When the weir height became large in the steady-state experiment, the froth height became also large. Similarly, the froth height increased with MeOH for lower concentration than 2 wt%. However, it did not vary for high concentation of MeOH. From the results shown in Fig. 37, D_E are plotted in Fig. 38 against the surface tension, where σ_w is the surface tension of water. D_E does not vary so much with surface tension except the range of σ/σ_w=0.95~1.0 for u=2000 and 3000 m/hr. As the results, the effect of surface tension on the eddy diffusivity is considered to be small. However, when the surface tension was decreased by adding the surface-active agent, the structure of froth was different from that of the aqueous MeOH solution. Therefore, concernig the effect of surface tension on the eddy diffusivity, a reliable conclusion is not yet obtained, and we are going to investigate it.

Chapter 6. Effect of phase change on plate efficiency

The plate efficiency or point efficiency which is the base of distillation efficiency have been investigated hitherto from a standpoint of mass transfer. However, in a practical distillation column, the temperature differs from plate to plate, and the condensation and vaporization are repeated at a local point in the vapor-liquid contacting layer. Therefore, the mass transfer on the plate is accompanied with the phase change which is caused by the heat transfer. The heat and mass transfer coefficients for the condensation were investigated in a wetted wall column whose surface area are known accurately. Using the results, the effect of phase change on the point efficiency is discussed in this section.

6. 1. Heat transfer coefficient for condensation[36, 43]

When the saturated vapor contacts with the saturated liquid, it is considered that the rate of phase change is controlled by the heat transfer in liquid near the interface. Then, the heat transfer coefficients were measured for the condensation of the saturated vapor of MeOH on the surface of wetted wall. In this case, the temperature in vapor-phase is uniform, and the temperature gradient is appeared only in liquid-phase. The results are shown in Fig. 39 with the results of literature.

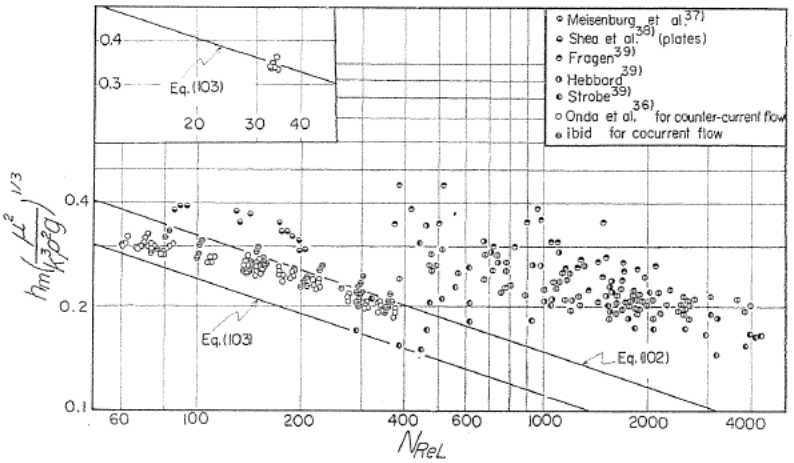

Fig. 39. Data for vapor condensation on vertical tubes.

When no liquid is fed at the top of column, the heat-transfer coefficient for the film condensation is given by rearranging Nusselt's equation as follows.

$$h_m\{\mu_L^2/(k_L^3\rho_L^2 g)\}^{1/3}=1.47(4\Gamma_b/\mu_L)^{-1/3} \qquad (102)$$

where h_m is the heat-transfer coefficient for the average film thickness [kcal/m²·hr·℃], k_L the thermal conductivity of liquid [kcal/m²·hr·℃], g the gravitational

acceleration [m/hr^2] and Γ_b the liquid flow rate per unit perimeter at the bottom of column [kg/hr·m]. On the other hand, when liquid is fed at the top of column, the heat-transer coefficient is expressed approximately dy

$$h_m\{\mu_L^2/(k_L^3\rho_L^2 g)\}^{1/3}=1.10(4\overline{\Gamma}/\mu_L)^{-1/3} \tag{103}$$

where $\overline{\Gamma}$ is the mean value of liquid flow rates at the top and bottom of column. In Fig. 39, our experimental values are larger 5~30% and 5~50% for the counter-current flow of vapor and liquid and the cocurrent flow respectively than those given by Eq. (103). These deviations are the same as those of experimental values by Shea[38] from Eq. (102). The deviation between the experimental and theoretical values increases with the increase of vapor velocity.

When Reynold's number N_{ReL} $(=4\Gamma/\mu_L)$ of liquid is larger than about 30, ripples are observed on the surface of liquid film in the wetted wall column. It is considered that the heat-transfer coefficient for the film condensation is reciprocal to the film thickness, and the following relation is derived by modelling ripples as shown in Fig. 40.

$$\frac{h}{h_m}=\delta_m\left\{\frac{1}{2}\frac{1}{\delta_{min}}+\int_0^{1/2}\frac{dx}{2(\delta_{max}-\delta_{min})x+\delta_{min}}\right\}$$
$$=1/(2X)+ln(Y/X)/\{2(Y-X)\} \tag{104}$$

where h is the heat-transfer coefficient, δ the film thickness, δ_m the average film thickness, $X=\delta_{min}/\delta_m$, and $Y=\delta_{max}/\delta_m$. From the holdup of the liquid film, $X=(4-Y)/3$ is obtained. Using the experimental values of δ_{max} in litarature[40], Eq. (103) is corrected by Eq. (104) and shown in Fig. 41 with a line (a). The line (b) in this figure is given by Dukler[41] for the heat-transfer

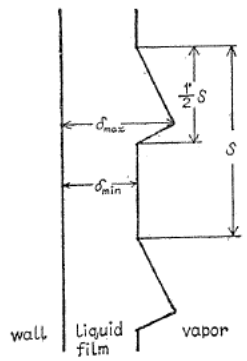

Fig. 40 Model of ripples.

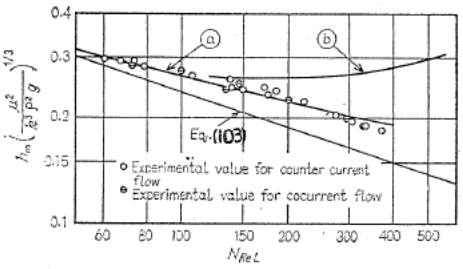

Fig. 41. h_m $(\mu^2/k^3\rho^2 g)^{1/3}$ vs. N_{ReL} for low vapor velocity.

coefficient of condensation. The experimental values plotted in Fig. 41 for low vapor velocity agree with the line (a). Therefore, taking into account the ripples on the surface of liquid film, the theoretical value of heat-transfer coefficient

coincides with the experimental one.

When vapor flow parallel to liquid, the momentum transfer through the interface affects the film thickness, i. e., the heat-transfer coeffient. Taking into account this effect, the local heat-transfer coefficient for a short section l in the direction of liquid flow is given as follows.

$$h_{loc}=\{1/(l\Delta T)\}[\{\delta_{out}/(6\mu_L)\}\{\pm 2Bu + \sqrt{(Bu)^2+16ACl+4A^2\delta_{in}^4}\pm 4ABu\delta_{in}^2 - \Gamma h_\lambda] \quad (105)$$

where

$$\delta=\sqrt{\mp Bu+\sqrt{(Bu)^2+16ACx+4A^2\delta_{in}^4}\pm 4ABu\delta_{in}^2/(2A)} \quad (106)$$

$A=h_\lambda\rho_L^2 g$, $B=\rho_L k_L \Delta T$, $C=\mu_L k_L \Delta T$, ΔT the temperature difference between vapor phase and wall, δ_{in} and δ_{out} are the film thicknesses at the inlet and outlet of this section, u the vapor velocity [m/hr], h_λ the heat of vaporization [kcal/kg], and x the distance on the section in the direction of liquid flow. The upper part of complex symdol represents the cocurrent flow and the lower part represents the counter-current flow. The ratios of the experimental heat-transfer coefficients to the theoretical ones calculated by Eqs. (104) and (105) are plotted against N_{ReV} $(=\rho_v ud/\mu_v)$ in Fig. 42, where d is the diameter of column. These points for both

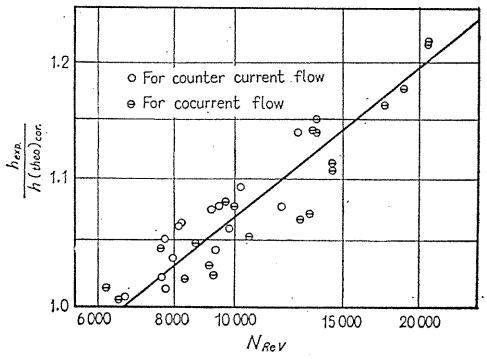

Fig. 42. $h_{exp}/h_{(theo)cor}$ vs. N_{ReV}.

the cocurrent and counter-current flows are correlated with a single line, and expressed as follows.

$$h_{loc}=\{1/(l\Delta T)\}[\{\delta_{out}/(6\mu)\}\{\pm 2Bu + \sqrt{(Bu)^2+16ACl+4A^2\delta_{in}^4}\pm 4ABu\delta_{in}^2\} - \Gamma h_\lambda] \times\{0.271(N_{ReV})^{0.17}\} \quad (107)$$

Although the values calculated by semi-theoretical Eq. (107) agree with the experimental values within 3 % error, Eq. (107) is complex and troublesome for use.

More simple correlations for the heat-transfer coefficients of condensation are given as follows.

$$N_{cond}=0.147(N_{ReL})^{-0.2}(N_{ReV})^{0.17} \tag{108}$$

for $20<N_{ReL}<150$, $7000<N_{ReV}<20000$,

$$N_{cond}=0.298(N_{ReL})^{-1/3}(N_{ReV})0^{0.17} \tag{109}$$

for $150<N_{ReL}<400$, $7000<N_{ReV}<20000$, where N_{cond} is the condensation number, $h\{\mu_L^2/(k_L^3\rho_L^2 g)\}^{1/3}$. N_{cond} varies very little with N_{ReV} in the range $N_{ReV}<7000$. The heat-transfer coefficients calculated by Eqs. (108) and (109) agree witn the experimental values within 5 % error as shown in Fig. 43.

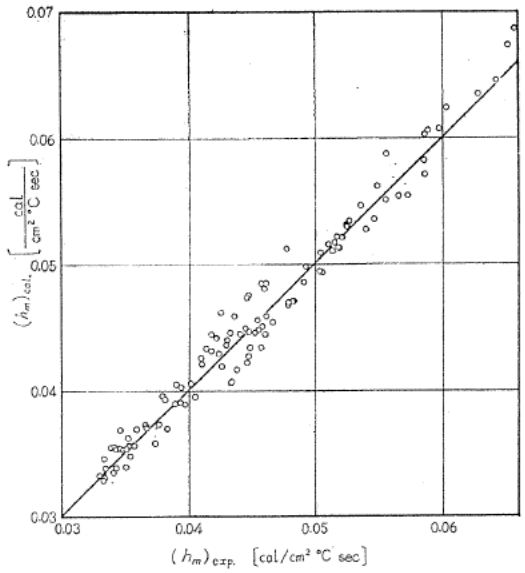

Fig. 43. Heat transfer coefficients calculated from Eqs. (108) and (109) vs. experimental heat transfer coefficients.

In the condensation of saturated vapor composed of one component, the temperature in vapor phase is uniform. However, in the condensation of mixed vapor, the temperature gradient is appeared in vapor phase as shown in Fig. 44. In this case the heat flux q_w through the wall is given as a sum of latent heat q_λ evolved at the interface by the condensation and q_v transfered from vapor phase by the convection. It can be written as follows[42].

$$q_w=q_\lambda+q_v=N_t h_\lambda M+\{h_g(T_v-T_i)a\}/(1-e^{-a}) \tag{110}$$

where $a=N_tC_p/h_g$, N_t the rate of condensation [kg-mole/m²·hr], M the molecular weight, h_g the heat-transfer coefficient in gas phase [kcal/m²·hr·°C], T_v and T_i the temperatures of vapor and interface respectively, and C_p the specific heat

[kcal/kg-mole·°C]. In the experiment[43] of the condensation of MeOH-wator vapor, q_v is that of order of 10 kcal/m²·hr and q_λ is that of order of 10^3 kcal/m²·hr. Thus almost all of heat flux through the wall will be ascribed to the latent heat evolved at the interface of the liquid film. It seems, therefore, that the resistance of liquid is controlling the heat transfer between vapor and wall.

In Fig. 45, q_λ is plotted against $(T_v - T_w)$ which is the temperature difference between the bulk of vapor and wall. The rate of condensation, that is, the liquid flow rate of the wall, is changed by varying the temperature difference $(T_v - T_w)$. The film thickness is proportional to the cubic root of liquid flow rate. Thus, the larger the flow rate is, the smaller the variation of film thickness. Therefore, when liquid is fed at the top of column, the thickness of liquid film, i. e., the resistance to the heat transfer does not change so much with the change of temperature difference $(T_v - T_w)$. In Fig. 45, the heat flux q_λ increases linearly with the increase of $(T_v - T_w)$ for each N_{ReV}. The straight line drawn in Fig. 45 is extended to the point where $q_\lambda = 0$, and the temperature difference ΔT_v is determined at this point. This value ΔT_v represents the temperature difference existing in the vapor phase. In the condensation of mixed vapor, q_v is neglected, and the heat-transfer coefficient of liquid film is given as follows.

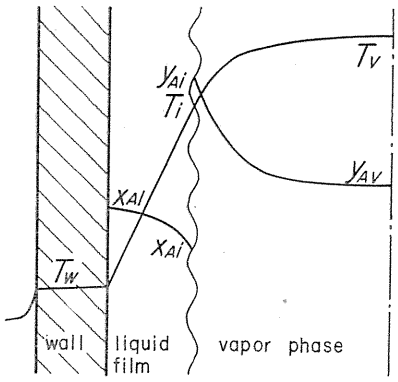

Fig. 44. Temperature and concentration profiles in the vapor phase and in the liquid film.

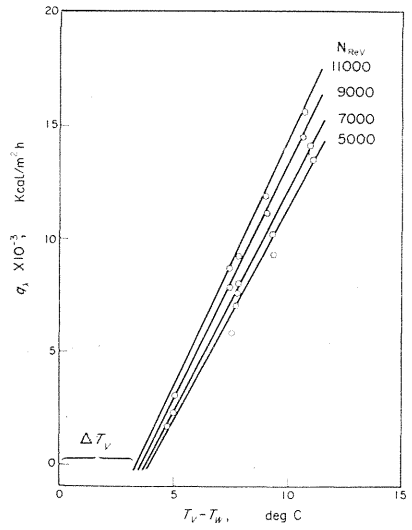

Fig. 45. Variation of the latent heat evolved at the vapor-liquid interface with temperature difference between vapor and wall.

$$h = q_\lambda / \{(T_v - T_w) - \Delta T_v\} \qquad (111)$$

With this heat-transfer coefficient, the condensation number is calculated with the physical properties of liquid in the film, and plotted against N_{ReL} in Eig. 46. Eqs. (108) and (109), which are the empirical equation obtained for the condesation of saturated pure vapor, and the theoretical Eq. (103) are shown with the solid lines in Fig. 46. The results of the condensation of mixed vapor agree with Eq. (108). Thus it will be concluded that the liquid film plays an important role in the condensation heat-transfer, and the condensation rate is controlled by the heat transfer in the liquid film, which can be treated in the same way for both the pure vapor and mixed vapor condensation.

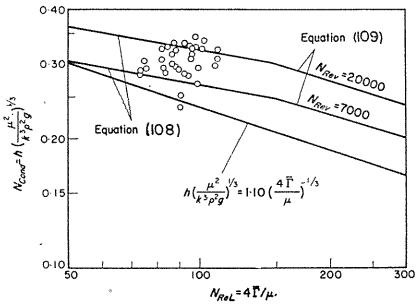

Fig. 46. Correlation of the condensation number with the liquid Reynold's number.

6. 2. *Mass transfer coefficients for mixed vapor condensation*[43]

In the case of a film condensation of mixed vapor on a wetted wall, the concentration profiles of more volatile component in the vapor phase and the liquid film are shown in Fig. 44.

When the mixed vapor is composed of only condensable components, the condensation rate is comparatively high and it will cause a bulk flow from the vapor phase to the interface. Since the bulk flow has considerable effect on the vapor-velocity profile and the concentration profiles in vapor and liquid phases, the problem must be treated as the high mass transfer-phenomenon.

The mass transfer coefficient k_y [kg-mole/m^2·hr·Δy] for the high mass transfer rates in vapor phase is defined as

$$N_{Ai}=-k_y(y_{Ai}-y_{Av})+y_{Ai}N_t \tag{112}$$

where N_{Ai} is a molar flux of more volatile component transferred through the interface. The mole fraction y_{Ai} in vapor at the interface is estimated from the assumption that the mixed vapor at the interface is saturated at temperature T_i $(=T_v-\Delta T_v)$. The mass-transfer coefficients k_y calculated by Eq. (112) are plotted against the condensation rate N_t in Fig. 47.

The value of k_y increases with the increase of N_t for each N_{ReV}, as shown in Fig. 47. To discuss the effect of condensation rate on the mass-transfer coefficients, the following relation is introduced.

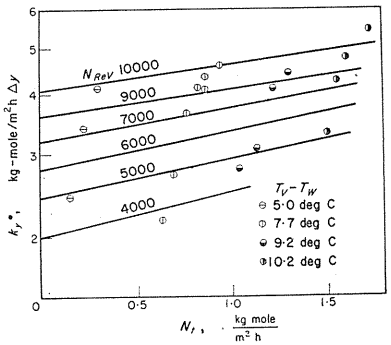

Fig. 47. Mass-transfer coefficients in vapor phase plotted against the condensation rate.

$$k_y=\lim_{N_t\to 0}k_y \tag{113}$$

The mass-transfer coefficient k_y obtained from Fig. 47 by Eq. (113) is one for the limiting condition in which the effect of bulk flow on the velocity and concentration profiles is neglected. The ratio θ of mass-transfer coefficients (k_y/k_y) calculated from the experimental data is plotted against Φ $(=N_t/k_y)$ in Fig. 48.

The relation between θ and Φ is derived on the basis of the film theory as

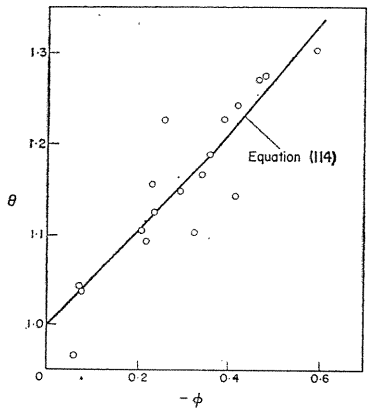

Fig. 48. Relation between θ and Φ for the mass transfer in vapor phase.

follows.

$$\theta=\Phi/(e^{\Phi}-1) \qquad (114)$$

This relation is shown by a solid line in Fig. 48. The agreement between the experimental data and the theory is satisfactory. Therefore, it will be concluded that the effect of condensation rate on the mass-transfer coefficient in vapor phase can be evaluated on the basis of the film theory.

On the basis of the film theory, the mass-transfer coefficient k_y for the condensation of mixed vapor is defined by Colburn-Drew[42] as follows.

$$N_t=k_y ln\{(z-y_{Ai})/(z-y_{Av})\} \qquad (115)$$

where $z=N_{Ai}/N_t$. k_y in Eq. (115) is the same as that defined by Eq. (113). The mass-transfer coefficients k_y are calculated by Eq. (115) with the same data as shown in Fig. 47, and plotted against N_{ReV} in Fig. 49. For all the temperature differences (T_v-T_w), the plotted data lie on a straight line.

In the liquid film, the bulk flow from the interface into the liquid-phase is caused by the condensation, and affects the concentration profile in liquid. The liquid phase mass-transfer coefficient k_x' is defined in the same way as k_y' by

$$N_{Ai}=k_x'(x_{Ai}-x_{Al})+N_t x_{Ai} \qquad (116)$$

Under the assumption that liquid at the interface is saturated at temperature T_i, the mass-transfer coefficients k_x' are calculated by Eq. (116) from the experimental data and plotted against N_t in Fig. 50. The value of k_x' decreases largely with the increase of N_t.

The local mass-transfer coefficient $k_{x,loc}'$ for the high mass-transfer rate is given as follows on the basis of the penetration theory.

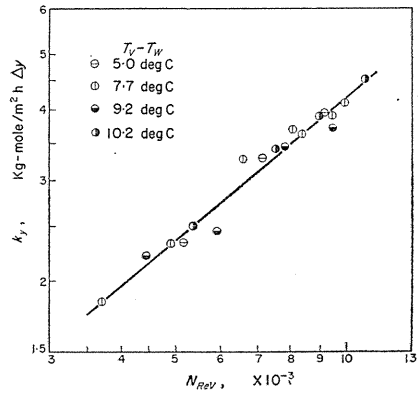

Fig. 49. Mass transfer coefficients in vapor phase calculated with Eq. (115).

$$k_{x,loc}'=N_t/[\sqrt{\pi}\Psi\{exp(\Psi^2)\}\{1+erf(\Psi)\}] \qquad (117)$$

where

$$\Psi=(N_t/C)\sqrt{t/D_L} \qquad (118)$$

C is the molar concentration [kg-mole/m³]. In the case of the condensation of

vapor in a wetted wall column, the contacting time t of liquid with vapor is given on an assumption that the condensation rate N_t is nearly uniform at any point of interface, as follows.

$$t=[24\rho_L\mu_L/\{g(N_tM)^3\}]^{1/3}\{(\Gamma_0+N_tMl)^{1/3}-\Gamma_0^{1/3}\} \qquad (119)$$

where Γ_0 is the liquid flow rate at the top of column. For each experimental condition the theoretical value of $k_{x,loc}^{\circ}$ is calculated from Eqs. (117) ~ (119), and averaged over the total length L_w of the column by

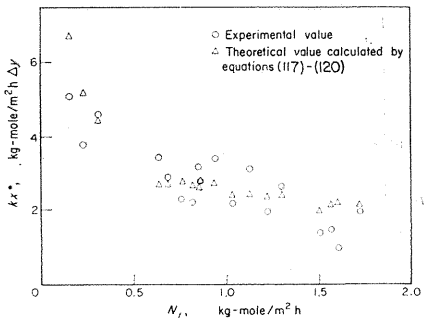

Fig. 50. Comparison of the experimental mass-transfer coefficients in the liquid film with theoretical values.

$$k_x^{\circ}=\frac{1}{L_w}\int_0^{L_w}k_{x,loc}^{\circ}dl \qquad (120)$$

The calculated results are shown in Fig. 50 as the theoretical values, and they agree with the experimental mass-transfer coefficients. Thus, the effect of condensation rate on the mass-transfer coefficient in liquid phase can be evaluated on the basis of the penetration theory.

The mass-transfer coefficient k_y° in vapor phase increases with the increase of the condensation rate as shown in Fig. 47. On the other hand, the mass-transfer coefficient k_x° in liquid phase decreases with the increase of the condensation rate as shown in Fig. 50. Therefore, the larger the condensation rate of mixed vapor is, the more important the role of the liquid resistance to the mass transfer is.

6. 3. *Effect of phase change on point efficiency*[44]

In the distillation column, the temperature falls from the bottom to top of column. When vapor contacts with liquid on a plate, the temperature of vapor entering from the under plate is higher than that of liquid on the plate. Therefore, the heat transfer from vapor to liquid phase occurs at the begining of contact. Since the rate of heat transfer in the liquid phase is higher than that in the vapor phase, vapor is considered to condense at the interface, and the bulk of liquid becomes super-heated state because of the heat transfer from the interface. Therefore, the condensation rate is lowered, and the vaporization cancelling the super-heated state occurs. Thus, it is considered that in the distillation process the condensation and vaporization are repeated on the plate. The effect of these phase change on the point efficiency is investigated by assuming the following model of vapor-liquid contact.

The vapor entering the plate rises as the bubble around which the liquid film is accompanied, and the condensation at the beginning of contact (for 1/10 of total contacting time) and the vaporization at the remaining contacting time occurs. Total quantity of condensation is equal to that of vaporization on a plate. When the condensation occurs, the heat evolved at the interface transfers into liquid and the temperature difference between vapor and liquid appears in liquid near the interface. The effects of phase change on the mass-transfer coefficients in the

vapor and liquid phases are expressed on the basis of the film and the penetration theories respectively.

The average rate of condensation is given by expressing the heat transfer in liquid from penetration theory, as follows.

$$\bar{N}_t=\bar{q}/h_\lambda=(2\Delta T/h_\lambda)\sqrt{k\rho C_p/(\pi t)} \tag{121}$$

On the other hand, the rate of vaporization is given as $\bar{N}_t'=\bar{N}_t/9$ from the ratio of contacting times. The effect of phase change on the mass-transfer coefficient in vapor phase is given by Eq. (114), and that in liquid phase is derived from Eq. (117) as follows.

$$k_{x,\,loc}'/k_{x,\,loc}=1/[\{exp(\Psi^2)\}\{1+erf(\Psi)\}] \tag{122}$$

The ratios of k_y'/k_y and k_x'/k_x calculated by Eqs. (114) and (122) respectively are shown in Fig. 51 for various temperature differences ΔT between vapor and liquid.

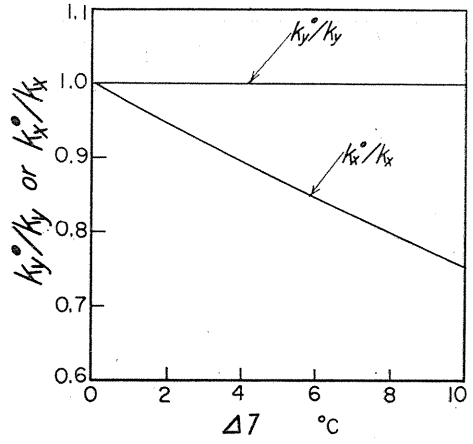

Fig. 51. Effects of temperature difference between vapor and liquid on the mass-transfer coefficients.

The conditions used in this calculation are selected by taking into consideration of the practical distillation system as follows: $h_\lambda=7000$ kcal/kg-mole, $k=0.14$ kcal/m²·hr·℃, $\rho=800$ kg/m³, $C_p=0.5$ kcal/kg·℃, $t=0.4$ sec, $k_y=10$ kg-moles/m²·hr, $C=10$ kg-moles/m³, and $D_L=5\times10^{-5}$ cm²/sec. From Fig. 51, the vapor-phase mass-transfer coefficient is affected very little by the phase change, and the considerably large effect of phase change is found for the liquid-phase mass-transfer coefficient.

The relation between the point efficiency and the transfer units is given by

$$-\frac{1}{in(1-E_{OG})}=\frac{1}{N_{OG}}=\frac{1}{N_G}+\frac{\lambda}{N_L} \tag{123}$$

where N_{OG} is the overall transfer unit based on the vapor composition, N_G the vapor-phase transfer unit, and N_L the liquid-phase transfer unit. The transfer units N_G and N_L are proportional to k_y and k_x respectivey. From the results in Fig. 51, the ratios between E_{OG}' and E_{OG} which are the point efficieneies with the phase

change and no phase change respectively, are shown in Fig. 52. When the mass transfer resistance in vapor phase is controllng, i. e., the small value of $N_G/(N_L/\lambda)$,

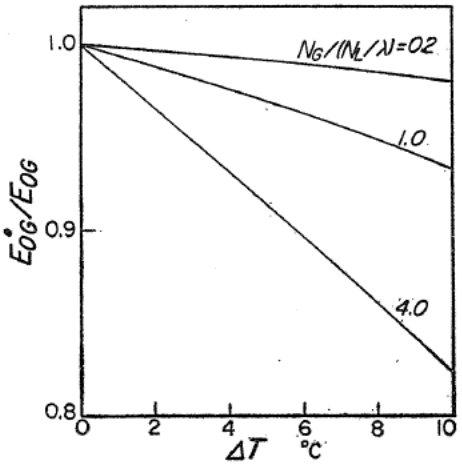

Fig. 52. Effects of phase change on the point efficiencies.

the effect of phase change on the point effciency is small, but it becomes large with the increase of $N_G/(N_L/\lambda)$. From Eq. (15), the plate efficiency becomes small with the increase of the relative volatility. It is considered that the effect of phase change is included in this decrease of the plate efficiency with the relative volatility, because the temperature difference from plate to plate increases generally with the increase of relative volatility.

Conclusion

The defects of murphree's plate efficiency has been clearly pointed out and the plate efficiency is newly defined under the assumption that vapor on an ideal plate is in equilibrium with liquid at the center of plate, The reflux ratio and the liquid mixing on the plate have little effects on the plate efficiency newly defined, and the efficiency is nearly equal to the point efficiency for the usual distillation conditions. The correlation for the plate efficiencies is given by Eq. (15) as a function of dimensionless variables.

Under the same assumption as used in the definition of plate efficiency, a graphical method to calculate the number of distillation plates for binary system is proposed by taking into account the liquid mixing on the plate, a step-to-step calculation for multicomponent system is also given. The relation between the column and plate efficiencies is derived as Eq. (79), and the relation between the plate efficiency based on the liquid composition and that based on the vapor composition is given by Eq. (86).

The eddy difusivities, which play an important role in the calculation of the number of plates, are correlated by Eq. (100) for the operating and design varia bles, and they decrease with the increase of liquid viscosity. Since the phase change

at a local point on the plate largely affects the liquid-phase mass-transfer coefficient, in the prediction of plate efficiency, the effect of phase change should be taken into account for the systems in which the mass-transfer resistance in liquid phase is controlling and the relative volatility is very large.

Literature cited

1) Lewis, W. K. Jr., *Ind. Eng. Chem.*, **28**, 399 (1936)
2) Onda, K., H. Takeuchi and K. Takahashi, *Joryu Gijutsu*, **3**, No. 3, 17 (1973)
3) *ibid*, **3**, No. 4, 23 (1974)
4) *ibid*, **4**, No. 1, 7 (1974)
5) *ibid*, **4**, No. 2, 35 (1974)
6) Marshall, W. R. Jr., and R. L. Pigford, "The Application of Differential Equations to Chemical Engineering Problems", p. 9, Univ. of Delaware, Delaware (1947)
7) Onda, K., Chem. Eng. (Japan), Ist Symposium, Dec. 1 (1962)
8) Onda, K. and O. Kobayashi, *Kagaku Kogaku*, **28**, 823 (1964)
9) Gautreaux, M. F. and H. E. O' Connell, *Chem. Eng. Progr.*, **51**, 232 (1955)
10) Anderson, J. E., Sc. D. thesis, Mass. Inst. Technol., Cambridge (1954)
11) Warzel, L., Ph. D. thesis, Univ. of Michigan (1955)
12) Onda' K., E. Sada, K. Takahashi and S. A. Mukhtar, *AIChE Journal*, **17**, 1141 (1971)
13) AIChE Res. Comm., "Tray Efficiencies in Distillation Columns", Final Rept., Univ. Delaware (1958)
14) AIChE Res. Comm., "Tray Efficiencies in Distillation Columns", Final Rept., State Collage N. Carolina (1959)
15) AIChE Res. Comm., "Tray Efficiencies in Distillation Columns", Final Rept., Univ. Mich. (1960)
16) Drickamer, H. G. and J. R. Bradford, *Trans. A. I. Ch. E.*, **39**, 319 (1943)
17) O' Connell, H. E., *Trans. A. I. Ch. E.* **42**, 741 (1946)
18) Umholtz, C. L. and M. Van winkle, *Ind. Eng. Chem.*, **49**, 226 (1957)
19) English, G. E. and M. Van Winkle, *Chem. Eng.*, **70**, 241 (1963)
20) Manning, E., Jr., S. Marple and G. P. Hinds, Jr., *Ind. Eng. Chem.*, **49**, 2051 (1957)
21) Rhodes, F. H. and P. G. Slachman, *Ind. Eng. Chem.*, **29**, 51 (1938)
22) McCabe, W. L. and E. W. Thiele. *Ind. Eng. Chem.*, **17** 605 (1925)
23) Fenske, M. R., *Ind. Eng. Chem.*, **24**, 482 (1932)
24) Onda, K., E. Sada, K. Takahashi and S. A. Mukhtar, *AIChE Journal*, **17**, 1147 (1971)
25) Onda, K., H. Takeuchi and K. Takahashi, *J. Chem. Eng. of* Japan, **5**, 13 (1972)
26) Onda, K., H. Takeuchi, K. Takahashi and H. Matsuoka, *J. Chem. Eng. of Japan*, **7**, 387 (1974)
27) Foss, A. S., J. A. Gerster and R. L. Pigford, *AIChE Journal*, **4**, 231 (1958)
28) Barker, P. E. and M. F. Self, *Chem. Eng. Sci.*, **17**, 541 (1962)
29) Harada, M., M. Adachi, W. Eguchi and S. Nagata, *Kagaku Kogaku*, **26**, 856 (1962)
30) Miyauchi, T., H. Imai and K. Kubo, *Kagaku Kogaku*, **30**, 643 (1966)
31) Gilbert, T., *Chem. Eng. Sci.*, **10**, 243 (1959)
32) Matsunaga, K., M. S. thesis, Nagoya Univ. (1973)
33) Matsuoka, H., M. S. thesis, Nagoya Univ. (1974)
34) Kafarov, V. V., V. V. Shestopalov and V. P. Belkov, *Int. Chem. Eng.*, **12**, 257 (1972)
35) DeGoederen, C. W. J., *Chem. Eng. Sci.*, **20**, 1115 (1965)
36) Onda, K., E. Sada, K. Takahashi and K. Ito, *Kagaku Kogaku*, **32**, 1215 (1968)
37) Meisenburg, S. J., R. M. Boorts and W. L. Bader, *Trans. A. I. Ch. E.*, **31**, 622 (1935)
38) Shea, F. L. and N. W. Krase, *Trans. A. I. Ch. E.*, **36**, 463 (1940)
39) McAdams, W. H., "Heat Transmission", McGraw-Hill (1954)
40) Kirkbride, C. G., *Trans. A. I. Ch. E.*, **30**, 170 (1934)

41) Dukler, A. E., Chem. Eng. Progr. Symp. Series, **56**, 1 (1960)
42) Colburn, A. P. and T. B. Drew, *Trans. A. I. Ch. E.*, **33**, 197 (1937)
43) Onda, K., E. Sada and K. Takahashi, *J. Heat Mass Transfer*, **13**, 1415 (1970)
44. Onda, K, H. Takeuchi and K. Takahashi, presented to *J. Heat Mass Transfer*.